

# Imaginary components of out-of-time correlators and information scrambling for navigating the learning landscape of a quantum machine learning model

Manas Sajjan<sup>†,1</sup> Vinit Singh<sup>†,1</sup> Raja Selvarajan,<sup>2</sup> and Sabre Kais<sup>1,2,3,\*</sup>

<sup>1</sup>Department of Chemistry, Purdue University, West Lafayette, IN 47907

<sup>2</sup>Department of Physics and Astronomy, Purdue University, West Lafayette, IN 47907

<sup>3</sup>Department of Electrical and Computer Engineering, Purdue University, West Lafayette, IN 47907

We analytically illustrate that the imaginary components of out-of-time correlators can be related to conventional measures of correlation like mutual information. We further rigorously establish the inherent mathematical bounds on such quantities respected by the dynamical evolution during training and explicate how the mere existence of such limits can be exploited to identify phase transitions in the simulated physical system using the quantum machine learning model. Such an analysis offers important insights into the training dynamics by unraveling how quantum information is scrambled through such a network introducing correlation among its constituent sub-systems. This approach not only demystifies the training of quantum machine learning models but can also explicate the capacitive quality of the model.

Heralding machine learning algorithms to be the most disruptive technological advancement of the present era would not be an overstatement [1–4]. Even though successful inroads of the former to enable scientific applications on both classical and quantum hardware have been demonstrated [5–11], the pervasive reluctance in making such algorithms mainstream can be attributed to the obscurity in the underlying learning process as indicated in a recent survey [12]. A part of the culpability is in the very paradigm of the training itself which seems often agnostic to physical principles or human-acquired domain intuition. Attempting to address this lacuna, the primary objective of our thesis is to gain physical insight into the learning mechanism of a machine learning model (to be called the learner) assigned to mimic the eigenstates of any user-defined system (to be called the driver), a task central to the core of many physico-chemical applications [13]

The major contributions of this work are many-fold. Following a description of the learner, we explicate the role of the information transport and scrambling between the internal sub-units of the learner during the course of its training. To this end, the hitherto unexplored imaginary component of out-of-time correlators (OTOCs)[14] of the learner is defined and analytically characterized using invariants of motion generated from the underlying Lie Algebra [15]. It is then subsequently employed to act as a compass in navigating the parameter landscape during learning. In recent years OTOCs has been used as a quintessential measure of how fast information propagation away from the source of initiation happens in the real-time post any local excitation in atomic systems [16–19], in statistical physics to probe thermalization [20–22], in quantum-information theory[23, 24], as a diagnostic tool for quantum chaos [25] and even in models mimicking aspects of quantum gravity [26–29]. Such correlators have also been measured using quantum circuits[30–34]. We thereafter connect such a quantifier with known measures of correlation and illustrate analytically the relative bounds shared by the two quantities, which are stricter than conventionally known bounds.

Equipped with these aforesaid probes, we then demonstrate with appropriate case studies how the footprints of correlation in the driver get imprinted onto a trained learner, thereby empowering the latter to be used as a concrete diagnostic tool in investigating physical phenomena like phase transitions as well as in differentiating between drivers with exotic connectivity/interactions, etc by simply accessing properties of the learner alone.

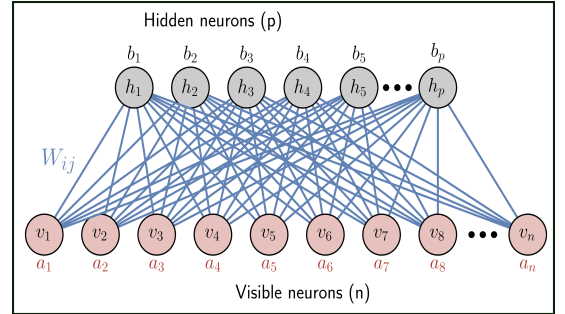


FIG. 1. The description of the learner network  $G = (V, E)$  as defined in text (also known as Restricted Boltzmann Machine (RBM) in literature[35, 36].) The set of hidden neurons  $\{h_j\}_{j=1}^p$  are shown in grey with the corresponding bias vector  $(\vec{b})$ . Similarly, set of visible neurons  $\{v_i\}_{i=1}^n$  are shown in red with the corresponding bias vector  $(\vec{a})$ . The interconnecting weight matrix with elements  $W_{ij}$  is shown in blue. The parameter set  $\vec{X} = (\vec{a}, \vec{b}, \vec{W})$  are tuned during the training of the network

The specific description of the generative network used as the learner in this work is illustrated in Fig.1. Formally the learner is a connected bipartite graph  $G = (V, E)$  (also known as Restricted Boltzmann Machine(RBM)[35–37]). The set  $V$  consists of all vertices (neurons) with  $|V| = (p + n)$  and  $(p, n) \in \mathbb{Z}_+$ . Any vertex  $v_i \in V$  is endowed with a locally accessible set  $S = (\hat{T}^i, x_i)$  where  $\hat{T}^i \in \{I(i), \sigma^x(i), \sigma^y(i), \sigma^z(i)\}$ , the usual Pauli operators, and  $x_i \in \mathcal{R}$ . Depending on the description of  $S$ ,  $v_i$  can be in either of the following two categories:

\* kais@purdue.edu

<sup>†</sup> These authors contributed equally to this work

$$v_i \in V = \begin{cases} v_i, & \text{if } \hat{T}^i = \sigma^z(v_i), x_i = a_i \\ h_i, & \text{if } \hat{T}^i = \sigma^z(h_i), x_i = b_i \end{cases} \quad (1)$$

where  $\sigma^z(\chi_i)$  with  $\chi \in \{v, h\}$  does not imply a functional dependence, but is a merely a marker that the  $\sigma^z$  is associated with the  $i$ -th neuron of node “ $\chi$ ”. This notation will be used throughout the text. The set of vertices  $V$  is thus characterized as  $V = \{v_i\}_{i=1}^{p+n} = \{v_i\}_{i=1}^n \cup \{h_j\}_{j=1}^p$ . The neurons of the type  $\{v_i\}_{i=1}^n$  (shown in red in Fig.1) collectively defines the visible spin-node register. If the hamiltonian matrix of the driver system is  $H \in \mathbb{C}^{d \times d}$ , then  $n = \lceil \log_2(d) \rceil$ . The neurons  $\{h_j\}_{j=1}^p$  (shown in grey in Fig.1) define the hidden-node register with  $p$  chosen arbitrarily by the user (usually  $p \sim n$ ).

The edge set  $E$  can be characterized with the adjacency matrix  $Adj(G) \in \{0, 1\}^{(n+p) \times (n+p)}$  of the graph  $G$  defined as follows:

$$Adj(G)_{ij} = \begin{cases} 1, & \text{if } v_i \in \{v_i\}_{i=1}^n, v_j \in \{h_j\}_{j=1}^p \\ & \forall (v_i, v_j) \in V \\ 0 & \text{otherwise} \end{cases} \quad (2)$$

$\forall (i, j) \in \mathcal{Z}^{p+n}$ . Corresponding to each non-zero entry in  $Adj(G)$  we define an edge  $e_{ij} \in E$ . This would mean that  $|E| = p * n$ . Associated with  $e_{ij} \in E$  we define a *weight* matrix  $\vec{W} \in \mathbb{R}^{n \times p}$  (shown in blue in Fig.1). Collectively the tunable parameters  $\vec{X} = (\vec{a}, \vec{b}, \vec{W}) \in \mathbb{R}^{n+p+n}$  enables us to define the learner’s Hamiltonian  $\mathcal{H} : G \mapsto \mathbb{R}^{2^{p+n} \times 2^{p+n}}$  similar to that of a classical Ising model [38, 39] as

$$\begin{aligned} \mathcal{H}(\vec{X}, \vec{v}, \vec{h}) &= \sum_{i=1}^n a_i \sigma^z(v_i) + \sum_{j=1}^p b_j \sigma^z(h_j) \\ &+ \sum_{i=1, j=1}^{n, p} W_j^i \sigma^z(v_i) \sigma^z(h_j) \end{aligned} \quad (3)$$

The network encodes a probability distribution which is essentially the diagonal elements of a thermal state  $\rho_{th}$ , of the corresponding Hamiltonian in Eq.3, and is defined as follows [36, 37, 40]:

$$\rho_{th}(\vec{X}, \vec{v}, \vec{h}) = \frac{e^{-\mathcal{H}(\vec{X}, \vec{v}, \vec{h})}}{\text{Tr}_{\{v, h\}} e^{-\mathcal{H}(\vec{X}, \vec{v}, \vec{h})}} \quad (4)$$

Any instance of spin configuration  $(\vec{v}, \vec{h})$  of the combined registers of  $(p+n)$  spins are samples drawn from the said thermal distribution in Eq.4. Equipped with this, the primary objective of the learner network  $G$  is to mimic the amplitude field of the target state  $\psi(\vec{X})$  of the driver hamiltonian  $H$  following the prescription

$$\psi(\vec{X}) = \sqrt{\sum_{\vec{h}} \text{diag}(\rho_{th}(\vec{X}, \vec{v}, \vec{h}))} \quad (5)$$

Whether the training happens on a classical processor or a NISQ device, the flow of the algorithm, in either case, involves randomly initializing  $\vec{X}$  to construct  $\psi(\vec{X})$  and then evaluating an appropriate merit-function  $J(\vec{X}) = \langle \hat{J} \rangle$  (usually  $\hat{J} = H$  but other properties can be optimized too). The variational parameters  $X = (\vec{a}, \vec{b}, \vec{W})$  are thereafter subsequently tuned using gradient-based updates of the merit function  $\partial_{\vec{X}} J(\vec{X})$  until a desired convergence threshold is reached. The algorithmic details of such a training process can be found elsewhere [41–44]. Formally such a training exploits the isomorphism of the vector space  $\mathbb{C}^d$  of the driver and the space of spin configurations  $S = \text{dim}(2^n)$  with  $n = \lceil \log_2 d \rceil$  of the learner as defined before. It must be emphasized that in this report we specifically treat instances wherein  $X \in \mathbb{R}^{p+n+p}$ . This dictates that Eq. 4, 5 are capable of simulating energy eigenstates of a driver  $H$  with non-negative coefficients only. The extension to the general case wherein the phase of the required eigenstate is tackled is straightforward [45, 46].

Having defined  $G$ , we posit the central thesis of the manuscript which is to probe into the training mechanism of the learner network described above using OTOCs. The primary component of any OTOC is two unitary operators  $U_1(t)$  and  $U_2(t)$  wherein  $U_i(0)$  is a local operator for a specific site  $i$  evolving in time  $t$  through Heisenberg prescription [47]. In recent literature, the following form for the OTOC has been indicated to be sensitive to the degree of information transport between sites  $\{1, 2\}$  and hence has been successfully used in a plethora of systems to quantify information scrambling[48–51]

$$C_{U_1, U_2}(t) = \langle U_1^\dagger(0) U_2^\dagger(t) U_1(0) U_2(t) \rangle \quad (6)$$

Unlike in most reports wherein the real part of Eq.6 is used, we offer in Appendix C a general formulation for obtaining the  $\text{Re}(C_{U_1, U_2}(t))$  and  $\text{Im}(C_{U_1, U_2}(t))$  through positive semi-definite construction of other appropriate operators. Intuitively  $C_{U_1, U_2}(t)$  measures the overlap between the state  $|U_1(0) U_2(t)\rangle$  and its dual with reversed order of operations. If the sites  $(1, 2)$  are far apart, the supporting bases of the operators  $U_1(0)$  and  $U_2(0)$  are sparsely-overlapping and hence  $C_{U_1, U_2}(0)$  will be 1. With time, the operator  $U_2(t) = e^{iH_{otoc}t} U_2(0) e^{-iH_{otoc}t}$  will start to extend its support under the effect of the generator  $H_{otoc}$  assuming the latter possesses interaction within the different sites of the system. This culminates in an eventual overlap between the probe operator  $U_1(0)$  and  $U_2(t)$  which leads to changing values of  $C_{U_1, U_2}(t)$ . The quantity  $C_{U_1, U_2}(t)$  thus directly hints at how fast the excitation has traveled from the initially localized point at 2 to site 1. The reason for the nomenclature of “out-of-time correlator” is due to the fact that the expression  $C_{U_1, U_2}(t)$  has a time-ordering which is non-monotonic as opposed to forward time correlators like  $\langle U_2(t) U_1(0) \rangle$  wherein the operators  $U_i$  are sequentially arranged in ascending order of time. Such two-point forward time correlators are not suitable for understanding information transport [52, 53] as they are known to decay and erase memory in  $O(1)$  time irrespective of the length ( $L$ ) of the system employed. This is in stark contrast to OTOCs which



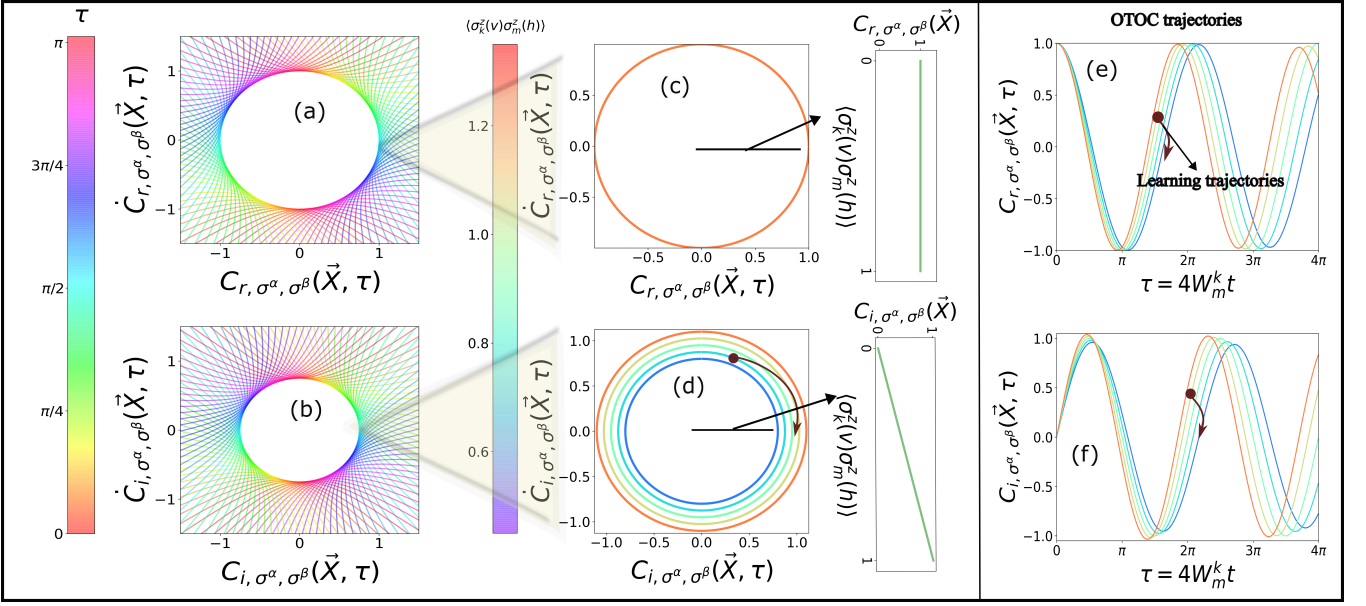


FIG. 2. (a) The profile for the invariant  $(\xi_{\sigma^\alpha,\sigma^\beta}(\vec{X},\tau)^2 - \xi_{\sigma^\alpha,\sigma^\beta}(\vec{X},\tau)^2) \cos(2\tau) + 2\xi_{\sigma^\alpha,\sigma^\beta}(\vec{X},\tau)\xi_{\sigma^\alpha,\sigma^\beta}(\vec{X},\tau)\sin(2\tau)$  obtained by combining Theorem .1 2(a) and Theorem .1 2(b) as  $\frac{I_1 I_2}{2}$  (see Appendix A) where  $\xi_{\sigma^\alpha,\sigma^\beta}(\vec{X},\tau) = \text{Re}(C_{\sigma^\alpha,\sigma^\beta}(0,0,\vec{X},\tau)) = C_{r,\sigma^\alpha,\sigma^\beta}(\vec{X},\tau)$  and  $\alpha = \beta = x$ . Note the subscript ‘r’ for the real part. As indicated, the quantity has been evaluated at  $(\kappa_1 = 0, \kappa_2 = 0)$ , hence the explicit dependence on  $(\kappa_1, \kappa_2)$  has been dropped in the latter symbol for notational brevity. For plotting the said invariant  $\tau = 4W_m^k t$  is used as the dependent variable. Each hyperbolic curve is the loci of points of the invariant with a fixed value of  $\tau$ . Sweeping  $\tau$  to explore the space may be administered by a variation in  $t$  or  $W_m^k$  (or both). The latter cases would naturally change  $\vec{X}$  too as  $W_m^k \in \vec{X}$ . The loci of all points with a fixed value of the invariant wherein  $\tau$  is changed solely due to  $t$  alone with  $W_m^k$  fixed (hence  $\vec{X}$  is fixed at say  $\vec{X}_0$ ) forms a circle at the center. (b) The profile for the invariant  $(\xi_{\sigma^\alpha,\sigma^\beta}(\vec{X},\tau)^2 - \xi_{\sigma^\alpha,\sigma^\beta}(\vec{X},\tau)^2) \cos(2\tau) + 2\xi_{\sigma^\alpha,\sigma^\beta}(\vec{X},\tau)\xi_{\sigma^\alpha,\sigma^\beta}(\vec{X},\tau)\sin(2\tau)$  obtained by combining Theorem .1 2(a) and Theorem .1 2(b) as  $\frac{I_1 I_2}{2}$  (see Appendix A) where  $\xi_{\sigma^\alpha,\sigma^\beta}(\vec{X},\tau) = \text{Im}(C_{\sigma^\alpha,\sigma^\beta}(0,0,\vec{X},\tau)) = C_{i,\sigma^\alpha,\sigma^\beta}(\vec{X},\tau)$  and  $\alpha = \beta = x$ . Note the subscript ‘i’ for the imaginary part. The exact same discussion about the latter notation and about the circle at the center holds true as in Fig.2(a) above. (c) The radius of the circle (demarcated in figure) from plot in Fig.2(a) is insensitive to  $\langle \sigma^x(v_k, 0), \sigma^x(h_m, 0) \rangle_{\rho_{th}(\vec{X}, \vec{v}, \vec{h})}$  (shown in color bar) and is simply a constant at 1 (see Eq.8) as also elaborated in the vertically arranged plot alongside. (d) The radius of the circle (demarcated in figure) from plot in Fig.2(b) is sensitive to  $\vec{X}$  as it is exactly equal to  $\langle \sigma^x(v_k, 0), \sigma^x(h_m, 0) \rangle_{\rho_{th}(\vec{X}, \vec{v}, \vec{h})}$  as also elaborated in the vertically arranged plot alongside (see Eq.8). This result thus indicates that the amplitude of the  $C_{i,\sigma^\alpha,\sigma^\beta}(\vec{X},\tau)$  can display information about the changing correlation content between the neurons of the visible and hidden node while  $\vec{X}$  changes during the training the network  $G$ , a result central to our thesis. (e) The harmonic behavior of  $C_{r,\sigma^\alpha,\sigma^\beta}(\vec{X},\tau)$  in real-time with the frequency equal to  $\tau$ . Note while training  $G$ , a typical learning trajectory in parameter space  $\vec{X}$  amounts to hopping from one such curve to another as indicated. (f) The harmonic behavior of  $C_{i,\sigma^\alpha,\sigma^\beta}(\vec{X},\tau)$  in real-time with the frequency equal to  $\tau$  and phase-shifted from Fig.2(e) by  $\frac{\pi}{2}$  (see Eq.8)

decay in time proportional to the difference in location of the two sites (hence  $\sim L$ ) [52] and also is extremely sensitive to the strength of the interaction between the two sites.

Using the aforesaid quantity, we can now probe how fast the learner network defined in graph  $G$  ‘learns’ and scrambles information between its constituent sub-systems. While from the optimization point of view, the role of the hidden set of neurons  $(\{h\}_{j=1}^p)$  is to enhance the expressive capability of the network by increasing the number of tunable parameters, from a more physical perspective  $\{h\}_{j=1}^p$  induces higher-order correlation between the neurons of the visible layer by relaying the information between a given  $(v_i, v_k) \in \vec{v}$  as the latter is devoid of any direct interaction. This relay is sensitive to the connections  $(e_{km} \in E)$  which defines the *weight* matrix elements  $W_{km}$  of the  $k$ -th neuron in  $\vec{v}$  and  $m$ -th neuron in  $\vec{h}$ . Thus testing how fast an initial excitation on a given visible neuron

is shared with a given hidden neuron in real-time will be a direct neuron-resolved picture of the dynamical evolution of the network during learning. To procure this insight, we define an OTOC with Pauli operators and establish the contents of the following theorem

**Theorem .1.** For a given parameter vector  $\vec{X}$ , one can define  $\mathcal{H}(\vec{X}, \vec{v}, \vec{h})$  (see Eq.3) and a thermal state  $\rho_{th}(\vec{X}, \vec{v}, \vec{h})$ . Let us thereafter define the following OTOC with  $U_1(0) = \tilde{\sigma}_\alpha = \sigma^\alpha(v_k, 0) - \kappa_1 \mathbf{I}$ , the time perturbed operator as  $U_2(0) = \tilde{\sigma}_\beta = \sigma^\beta(h_m, 0) - \kappa_2 \mathbf{I}$  and the generator  $H_{otoc} = \mathcal{H}(\vec{X}, \vec{v}, \vec{h})$  in Eq.6  $\forall \{\alpha, \beta\} \in \{x, y\}$ .

$$C_{\sigma^\alpha,\sigma^\beta}(\kappa_1, \kappa_2, \vec{X}, t) = \langle \tilde{\sigma}^\alpha(v_k, 0) \tilde{\sigma}^\beta(h_m, t) \tilde{\sigma}^\alpha(v_k, 0) \tilde{\sigma}^\beta(h_m, t) \rangle \quad (7)$$

Note that  $\{\kappa_1, \kappa_2\} \in \mathcal{C}^2$  are arbitrary user-defined mean trans-lations. Also  $\langle \cdot \rangle$  indicates averaging over the thermal state  $\rho_{th}(\vec{X}, \vec{v}, \vec{h})$  which activates the  $\vec{X}$  dependence. Using 7, one can then make the following statements:

$$1. C_{\sigma^\alpha, \sigma^\beta}(\kappa_1, \kappa_2, \vec{X}, t) = C_{\sigma^\alpha, \sigma^\beta}(0, 0, \vec{X}, t) + |\kappa_1|^2 |\kappa_2|^2 + |\kappa_2|^2 + |\kappa_1|^2$$

We thus see  $C_{\sigma^\alpha, \sigma^\beta}(0, 0, \vec{X}, t)$  is the key component in the expression for Eq.7

2. The following invariants of motion exists for  $C_{\sigma^\alpha, \sigma^\beta}(0, 0, \vec{X}, t)$ :

$$(a) I_1 = -2\xi_{\sigma^\alpha, \sigma^\beta}(\vec{X}, \tau) \cos(\tau) - \xi_{\sigma^\alpha, \sigma^\beta}(\vec{X}, \tau) \sin(\tau)$$

$$(b) I_2 = -2\xi_{\sigma^\alpha, \sigma^\beta}(\vec{X}, \tau) \sin(\tau) + \xi_{\sigma^\alpha, \sigma^\beta}(\vec{X}, \tau) \cos(\tau)$$

where  $\xi_{\sigma^\alpha, \sigma^\beta}(\vec{X}, \tau)$  can either be the real or the imaginary part of  $(C_{\sigma^\alpha, \sigma^\beta}(0, 0, \vec{X}, \tau))$  and  $\square$  is  $\frac{\partial \square}{\partial \tau}$  with  $\tau = 4W_m^k t$

*Proof.* See Appendix A  $\square$

A direct corollary of the contents of Theorem .1 (also proven in Appendix as Corollary A.0.2) is that one can easily deduce an analytical expression for  $C_{\sigma^\alpha, \sigma^\beta}(0, 0, \vec{X}, \tau)$  as

$$C_{\sigma^\alpha, \sigma^\beta}(0, 0, \vec{X}, \tau) = \cos(\tau) + i \langle \sigma^z(v_k, 0) \sigma^z(h_m, 0) \rangle_{\rho_{th}(\vec{X}, \vec{v}, \vec{h})} \sin(\tau) \quad (8)$$

Thus we see that the behavior of OTOC in Eq. 8, is oscillatory which can be rationalized using the fact that the generator  $H_{otoc}$  (in Eq. 3) consists of  $\sigma^z$  operations only which due to  $SU(2)$  algebra, unitarily rotates the eigenvectors of the  $\sigma^\beta(h_m, t)$  ( $\beta \in \{x, y\}$ ) operators in the definition for the OTOC (see Eq. 7) around the z-axis. This leads to the growth in the supporting sites of the operator culminating in a significant yet oscillatory overlap with  $\sigma^\alpha(v_k, 0)$ . The frequency associated with the rotation for both the real and the imaginary components in Eq. 8 is independent of the local biases ( $\vec{a}, \vec{b}$ ) but is expectedly dictated by the strength of the interaction ( $W_m^k$ ) between the  $k$ -th visible neuron and  $m$ -th hidden neuron. However an even more interesting observation is the fact that the amplitude of  $Im(C_{\sigma^\alpha, \sigma^\beta}(0, 0, \vec{X}, \tau))$  in Eq.8 yields directly a two-body correlation function  $\langle \sigma^z(v_k, 0) \sigma^z(h_m, 0) \rangle_{\rho_{th}(\vec{X}, \vec{v}, \vec{h})}$  of spins in the visible and hidden register of the learner. Since such functions are sensitive to the  $\vec{X}$ , they have the power to directly probe how the correlation content between the neurons of the systems  $\vec{\sigma}$  and  $\vec{h}$  changes in real-time as the training progresses. To consolidate this more concretely, one can establish a relationship with  $Cov(\sigma^x(v_k, 0), \sigma^x(h_m, 0))_{\rho_{th}}$  directly by combining the assertions of Theorem .1(1) and Eq.8

as follows

$$\begin{aligned} \eta(\vec{X}) &= Cov(\sigma^z(v_k, 0), \sigma^z(h_m, 0))_{\rho_{th}} \\ &= C_{\sigma^\alpha, \sigma^\beta}(\sqrt{i \langle \sigma^z(v_k, 0) \rangle}, 0, \vec{X}, \tau = \frac{\pi}{2}) \\ &\quad + C_{\sigma^\alpha, \sigma^\beta}(0, \sqrt{i \langle \sigma^z(h_m, 0) \rangle}, \vec{X}, \tau = \frac{\pi}{2}) \\ &\quad - C_{\sigma^\alpha, \sigma^\beta}(\sqrt{i \langle \sigma^z(v_k, 0) \rangle}, \sqrt{i \langle \sigma^z(h_m, 0) \rangle}, \vec{X}, \tau = \frac{\pi}{2}) \end{aligned} \quad (9)$$

$\eta(\vec{X})$  in Eq.9 can only attain a value of zero if the neurons  $v_k$  and  $h_m$  are uncorrelated. Having established this we shall now proceed to connect the said amplitude  $\eta(\vec{X})$  to well-known correlation measures like Von-Neumann entropies of the sub-systems and the incipient mutual information ( $I(v_k, h_m)$ ) [54–57]. To this end, we shall prove the following theorem

**Theorem .2.** For a given parameter set  $\vec{X}$ , associated with Eq.4, the two particle-density matrices  ${}^2\rho(v_k, h_m)$  and one particle-density matrix  ${}^1\rho(v_k)$  of the learner  $G$  can be computed. Using these one can construct  $I(v_k, h_m) = S({}^1\rho(v_k)) + S({}^1\rho(h_m)) - S({}^2\rho(v_k, h_m))$  where  $S(Y) = -Tr(Y \ln Y)$ . The following statement is true

$$LB \leq I(v_k, h_m) \leq UB \quad (10)$$

wherein the lower bound (LB) is

$$\begin{aligned} LB &= 2 + \left(\frac{1 + \eta(\vec{X})}{2}\right) \ln\left(\frac{1 + \eta(\vec{X})}{4}\right) \\ &\quad + \left(\frac{1 - \eta(\vec{X})}{2}\right) \ln\left(\frac{1 - \eta(\vec{X})}{4}\right) \end{aligned} \quad (11)$$

and the corresponding upper bound (UB) is

$$\begin{aligned} UB &= -\left(\frac{1}{2} + \frac{\sqrt{1 + (-1)^\gamma \eta(\vec{X})}}{2}\right) \ln\left(\frac{1}{2} + \frac{\sqrt{1 + (-1)^\gamma \eta(\vec{X})}}{2}\right) \\ &\quad - \left(\frac{1}{2} - \frac{\sqrt{1 + (-1)^\gamma \eta(\vec{X})}}{2}\right) \ln\left(\frac{1}{2} - \frac{\sqrt{1 + (-1)^\gamma \eta(\vec{X})}}{2}\right) \end{aligned} \quad (12)$$

with  $\eta(\vec{X})$  defined in Eq.9 and  $\gamma = 1$ , if  $\eta(\vec{X}) \geq 0$  or  $\gamma = 0$ , if  $\eta(\vec{X}) < 0$  and  $-1 \leq \eta(\vec{X}) \leq 1$

*Proof.* See Appendix B  $\square$

The implication of Theorem .2 is profound and is directly illustrated diagrammatically in Fig.3(a). To respect the relations between  $I(v_k, h_m)$  and  $\eta(\vec{X})$  above, Eq.11, 12 establishes for the first time the restrictions on physical quantifiers like  $I(v_k, h_m)$  which the RBM network  $G$  uses for representing a given state of the physical system defined by a given driver. The upper bound and the lower bound thus together define a convex set (see Fig 3(a)) within which resides the acceptable values of  $I(v_k, h_m)$  and  $\eta(\vec{X})$ , that the learner network can access during the course of its training. It must be noted, that

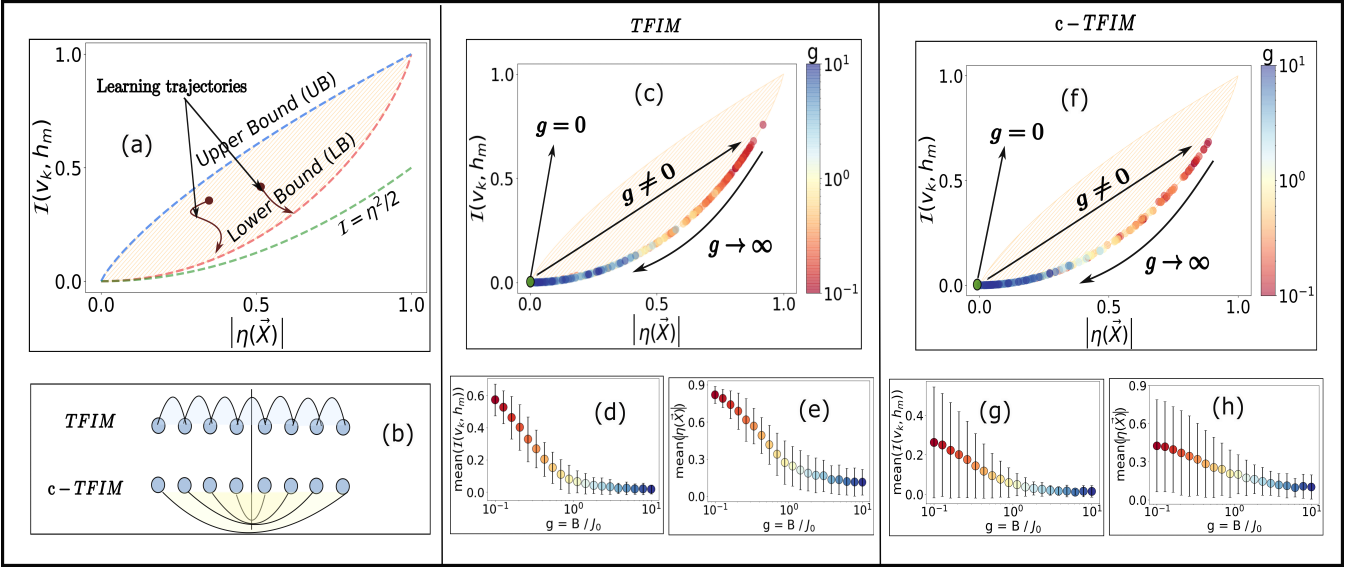


FIG. 3. (a) The upper bound(UB) and lower bound (LB) in the convex  $I - \eta$  space for network  $G$  as described in Theorem.2 in Eq.12 and Eq.11 respectively. In all plots in this panel we shall use  $\alpha = \beta = x$  in Eq.9. Provided alongside in green is the conventionally known lower bound for any general bi-partition of an arbitrary system [58]. The lower bound (LB) for  $G$  is thus stricter than the known general bound and collapses to the latter when  $\eta(\vec{X}) \rightarrow 0$ . Representative learning trajectories of the network  $G$  are shown. They involve changing the parameter  $\vec{X}$  thereby navigating the  $I - \eta$  space. (b) The schematics of the interactions among the spin registers in the area-law entangled ground state of the driver Hamiltonian defined in Eq.13(TFIM) [59–61] and for the volume-law entangled ground state of another driver system defined in Eq.14(c-TFIM) [62] (see text for more details). (c) The  $I(v_k, h_m)$  and  $\eta(\vec{X})$  values corresponding to the finally converged parameter  $\vec{X}$  of the trained network  $G$  for the ground state of Eq.13 as driver with  $N = 4$  (hence  $n = p = 4$  in  $G$ ). We see that the representations chosen by the trained network  $G$  in  $I - \eta$  space corresponding to a family of ground states with different values of  $g = \frac{B}{J_0}$  (shown in the color bar) always saturate the LB (Eq. 11) and slides along it monotonically for  $g \in (0, \infty]$ . For  $g = 0$ , the representation of  $G$  is also uncorrelated with a cluster of points near the green dot corresponding to the uncorrelated, two-fold degenerate ferromagnetic ground state ( $|0000\rangle$  or  $|1111\rangle$ ). For  $g \rightarrow 0_+$  however, the representation shifts dramatically (red points) as the ground state of the driver admits a superposition of several bit-strings. Enhanced correlation in the said ground state is manifested in the trained state of the network through the retention of correlation among the various pair of neurons ( $\forall (k \in [4], m \in [4])$  i.e. 16 pairs). For  $g \rightarrow \infty$ , the ground state of the driver is once again uncorrelated ( $|++++\rangle$ ) which consequently is mirrored in the representation of  $G$  with a steadily declining  $I(v_k, h_m)$  and  $\eta(\vec{X})$  (blue dots) among the various pair of neurons. (d) The plot of the mean of  $I(v_k, h_m)$  vs  $g$  from Fig.3(c) where the averaging is done not only over all pairs of  $(k, m)$  for a single run but also over many runs (to eradicate sensitivity to initialization which can affect convergence) at a given  $g$ . The standard deviation from the sample runs at each  $g$  is also indicated along with the mean. This plot bolsters the aforesaid points. (e) Similar plot as in Fig.3(d) but for  $\eta(\vec{X})$  consolidating the concomitant attenuation in the amplitude of the  $Im((C_{\sigma^\alpha, \sigma^\beta}(0, 0, \vec{X}, \tau)))$  as observed in Fig.3(c) before (f) The plot of  $I(v_k, h_m)$  and  $\eta(\vec{X})$  corresponding to the converged parameters of  $G$  for the ground state of c-TFIM (see Eq.14) as driver for different values of  $g$  (shown in color bar) for  $N = 4$  spins. The observations are similar to Fig.3(c). (g) Similar plot as in Fig.3(d) but for c-TFIM illustrating the decline of  $I(v_k, h_m)$  with enhancing  $g$ . However unlike in Fig.3(d) we see the corresponding standard deviations have increased considerably indicating many different consistent representations ( $\vec{X}$ ) of the trained network  $G$ . (h) Similar plot as in Fig.3(e) but for c-TFIM showing diminishing  $\eta(\vec{X})$  with increasing  $g$ . The same observation of enhanced standard deviation also applies. We thus see from Fig.3(c-h) that the correlation among the neurons of the fully trained network  $G$  in the  $I - \eta$  space can be used as a marker to infer/probe the existence of the different phases (like the ordered and disordered phases of TFIM for various  $g$ ) as well as to differentiate between ground states of volume-law entangled versus an area-law entangled systems.

training of the network in epochs is not similar to the real-time progression of the OTOC as illustrated in Fig.2(e-f). It is best to interpret the OTOC in Eq.7 as the quantifier for information scrambling between a hidden and a visible neuron in real-time for given a parameter  $X$  at a particular training step. The training trajectory on the other hand is traversing the parameter space from one point to another each of which is capable of generating an OTOC with the incumbent instance of  $\vec{X}$  as defined in Eq.7. We must also emphasize that LB in Eq.11 is more stringent and is specific to the network  $G$  compared to

previously known bound of  $\frac{\eta(\vec{X})^2}{2}$  [58] as seen in Fig.3(a). The difference is especially appreciable for larger regimes of  $\eta(\vec{X})$  explicating that the RBM network  $G$  admits a representation ( $\vec{X}$ ) which possesses larger  $I(v_k, h_m)$  than what would usually be permissible from bi-partitions.

To exemplify the direct consequences of Theorem .2, we now make use of the Transverse Field Ising model (TFIM) as

a driver. The Hamiltonian for the system is

$$H = -B \sum_{i_d}^N \sigma^x(i_d) - J_0 \sum_{i_d}^{N-1} \sigma^z(i_d) \sigma^z(i_d + 1) \quad (13)$$

where ( $B \geq 0, J_0 \geq 0$ ) defines the local on-site magnetic field and exchange spin coupling and  $i_d$  runs over the indices of the spins of the driver. We use  $N = 4$  spins for illustration. The interactions are schematically displayed for  $N = 8$  spins in Fig.3(b). The ground state of the system has non-negative coefficients as a consequence of the Perron-Frobenius theorem [63, 64]. Note Eq.13 defines a system of  $N$  spin- $\frac{1}{2}$  which is completely remote and oblivious to the spin registers of the network  $G$ . The latter serves to learn the ground state of Eq.13 using ( $n = N = 4, p = 4$ ) neurons for the visible and hidden register respectively by exploiting Eq.4 and Eq.5.

We define  $g = \frac{B}{J_0}$  as a control parameter to realize the phases of Eq.13. We run several numerical experiments with different randomly chosen initial parameters and train the network  $G$  to learn the ground state of Eq.13. The error threshold is set to  $\leq 10^{-3}$ . We show details of the training results in Appendix F. We use the parameter set at the final iteration of the best converged result (say  $X^* = (\vec{a}^*, \vec{b}^*, \vec{W}^*)$ ) to compute  $I(v_k, h_m)$  and  $\eta(\vec{X})$  and display the corresponding points in convex space of  $I - \eta$  in Fig.3(c). We note that representations chosen by the trained network for the ground state always saturate the lower bound  $LB$  (see Eq. 11). We further compute a representative center of mass of  $\eta(\vec{X})$  and  $I(v_k, h_m)$  by averaging over all  $(k, m)$  for a given run and also over many different crisply converged experiments/runs (to remove sensitivity against initial conditions) and report the sample mean and sample standard deviation in Fig. 3(d) and Fig.3(e) respectively.

Since we are using  $J_0 \geq 0$ , when  $g = 0$ , we have a ferromagnetic two-fold degenerate uncorrelated ground state [63]. This behavior is reflected in the  $I - \eta$  space as a cluster of points near (0,0) in Fig.3(c) (represented by a green dot). In this regime, the network  $G$  thus chooses a representation devoid of any correlation between sub-systems of the visible and hidden neurons  $\forall(k, m)$ . As soon as  $0 \leq g \leq 1$ , the driver system exhibits correlated behavior with the ground state being a superposition of many spin configurations. The corresponding network  $G$  mirrors this behavior too by now choosing a representation that has a significant correlation among the bi-partitions in visible and hidden neurons (red dots in Fig.3(c)) thereby escalating  $I(v_k, h_m)$  and  $\eta(\vec{X})$ . This is further reflected in the higher mean  $I(v_k, h_m)$  and higher mean  $\eta(\vec{X})$  than in the  $g = 0$  case in Fig.3(d), Fig.3(e). For  $g \rightarrow \infty$ , we also have an uncorrelated state with all spins in state  $\frac{|0\rangle + |1\rangle}{\sqrt{2}}$ . Thus the representation which the network  $G$  chooses moves steadily towards the (0, 0) point in  $I - \eta$  space (blue dots in Fig.3(c)) as  $g$  is raised. This is further corroborated in Fig.3(d) and Fig.3(e) which shows the respective mean declining steadily. The corresponding standard deviation in the latter two plots reflects the variance in the representation chosen by the network over various runs for a given  $g$  and shows a steady decrease indicating that the various

neurons unanimously reach a unique configuration in the large  $g$  limit devoid of correlations among bi-partitions described above. In this model, the phase transition from the ordered ferromagnet to the disordered phase happens due to spontaneous breaking of  $\mathbb{Z}_2$  symmetry ( $\sigma^z(i_d) \rightarrow -\sigma^z(i_d)$  or  $\pi$  rotation around  $\sigma^x(i_d)$ ) below  $g \leq 1$ . The critical point is  $g_c = 1$  in the thermodynamic limit but appears earlier in Fig.3(d), Fig.3(e) due to finite-size effects.

The model Hamiltonian in Eq.13 admits a ground state which possesses nearest-neighbor interactions only and hence is amenable to area-law-scaling in the Von-Neumann entropy (VNE) across a central bi-partition of the system. For 1D systems like TFIM with neighboring interactions only, since a constant number of bonds are broken with such partitions, VNE would be insensitive to the size of each sub-system creating a hallmark of area-law scaling. It has been reported in literature [65, 66] that initiating inhomogeneous connectivity  $J_{ij}$  among the spins with a power-scaling coefficient  $\alpha$  can only afford a weaker logarithmic correction in subsystem size to the VNE. However, to explore a true volume-law scaling we use next, an engineered spin-connectivity described in the literature as concentric-TFIM [67] (henceforth to be labeled as c-TFIM) for spin-chains with an even number of sites  $N$ . The hamiltonian for this driver system with spin indices  $(i_d, j_d)$  is (see also Fig. 3(b))

$$H = -B \sum_{i_d}^N \sigma^x(i_d) - \sum_{i_d j_d} J_{i_d j_d} \sigma^z(i_d) \sigma^z(j_d)$$

$$\text{where } J_{i_d j_d} = \begin{cases} J_0, & \text{if } i_d = \frac{N}{2} - (q - 1), \\ & j_d = \frac{N}{2} + q \\ 0 & \text{otherwise} \end{cases}$$

$$\text{with } \forall q \in [1, \frac{N}{2}] \quad (14)$$

The connectivity graph of Hamiltonian in Eq.14 necessitates that the number of bonds compromised on a central bi-partition of the system scales linearly in the size of each sub-system on either side of the partition. This ensures a volume-law scaling in VNE (see Fig. 3(b) for the schematic of the interactions in the case of  $N = 8$  spins. Also refer to Appendix G for direct corroboration). As in the case of TFIM, we use  $N = 4$  which ensures ( $n = N = 4, p = 4$ ). We run experiments with the same set of initial parameters and plot the converged results from the training in  $I - \eta$  space, in mean  $I(v_k, h_m)$  vs  $g$  and mean  $\eta(\vec{X})$  vs  $g$  wherein  $g = \frac{B}{J_0}$  as before. The respective results are plotted in Fig.3(f), Fig.3(g), Fig.3(h).

In all three figures, we see similar trend as in the previous case for TFIM i.e.  $I(v_k, h_m)$  and  $\eta(\vec{X})$  attenuating in the limit of  $g \rightarrow \infty$  when the system attains the uncorrelated configuration where all spins are in  $\frac{|0\rangle + |1\rangle}{\sqrt{2}}$ . However the signature of the volume-law entanglement is captured in the higher variance of the representations of the network  $G$  as seen in Fig.3(g) and Fig.3(h) for a given  $g$  compared to Fig.3(d) and Fig.3(e). This indicates that for a correlated volume-law entangled state



the network offers many different representations among various  $(k, m)$  as well as from different initial conditions thereby offering a wide variety of  $I(v_k, h_m)$  and  $\eta(\vec{X})$  values. This can act as a signature for detecting such a system using information from the training trajectories of the network  $G$  alone.

In this work, we established a number of key physical insights about the training of the learner network  $G$ . The choice of this specific network is attributed to its astonishing success in simulating a wide variety of quantum systems in condensed matter physics like strongly correlated fermionic assemblies [41, 68, 69], topologically non-trivial phases [70], anyonic symmetries [71], in quantum dynamical evolution [72], in chemistry like 2D-materials [13, 44, 73] and molecules with multi-reference correlation [74] under geometric distortion [45], and even in classification tasks [43, 75] with quantum or classical data. In fact,  $G$  has been proven to act as a universal approximator for any probability density [35, 76] thereby providing a guarantee to the range of its representational capacity. Prior work has also established that the network is capable of mimicking the amplitude of a  $2^n$  dimensional volume-law entangled quantum state even with a sparse representation [77] i.e. using  $O(n)$  parameters as opposed to  $O(mn)$  in the usual case. Ref [78] has established that the task of retrieving the full distribution encoded within  $G$  would always entail exponential classical resources unless the polynomial hierarchy collapses. However, quantum circuits to simulate the same with quadratic qubits and gate costs ( $O(mn)$ ) already exist. Another feature enjoyed by the network is its easy extension to  $d$ -dimensional spins [70] which makes encoding higher dimensional quantum states of a driver tractable.

Using such a widely recognized network, we have illustrated a thorough analysis of how changing correlation within the spins of the learner can be understood using imaginary components of OTOC and have analytically established its relationships with bipartite mutual information. We have further demonstrated for both volume and area-law entangled states that it is possible to infer the quality of phases in a given driver Hamiltonian (in this case Eq. 13 or Eq. 14) just by studying the representation of the corresponding learner  $G$  in the trained state by exploring the  $I - \eta$  space described above. Such a

study begins to probe into the rich underlying universe of the training mechanism and shows that the representations chosen by the learner during the training epoch are quantifiably tuned to re-adjust the correlation content among the pairwise bi-partitions of visible and hidden neurons commensurate with the changing quantum correlation in the actual driver system. This enables such representations to provide distinct markers like  $I(v_k, h_m)$  and  $\eta(\vec{X})$  which can be used to diagnose phase transitions in the driver. In Appendix H we provide another marker (largest eigenvalue of Fisher Information matrix constructed using the trained parameter set  $\vec{X}$  of the network  $G$ ) which is also capable of displaying tell-tale signs of phase transitions.

Our analysis can come to be useful in physics-inspired learning networks [79–81]. Further extension of our study may be to understand where in the  $I - \eta$  space do eigenstates of different interacting quantum matter lie and how can that information be leveraged while initializing the network  $G$  a priori to expedite the training. Although all results are analytically established, since direct measurement of OTOCs is a possibility even on a quantum circuit [30, 31], experimental measurement of the imaginary component of the OTOC string for our learner can be undertaken and its relationship with  $I$  be exploited. With the present-day promise of machine/deep learning, the authors hope that more such studies will be initiated which in spirit ‘humanizes’ already-established black-box models by probing into their learning universe, removes the shroud of mystery behind their training, and will hopefully lead to enhanced cross-pollination with physical sciences and ameliorated standards in model-development. The benefits of such a pipeline can surely be harvested to achieve unprecedented feats in simulating the natural world.

## ACKNOWLEDGMENTS

The authors would like to acknowledge the financial support of the U.S. Department of Energy, Office of Science, National Quantum Information Science Research Centers, Quantum Science Center, and the National Science Foundation under Award Number 1955907.

- 
- [1] A. Burkov, *The hundred-page machine learning book*, Vol. 1 (Andriy Burkov Quebec City, QC, Canada, 2019).
  - [2] I. H. Sarker, Machine learning: Algorithms, real-world applications and research directions, *SN Computer Science* **2**, 1 (2021).
  - [3] D. Dhall, R. Kaur, and M. Juneja, Machine learning: A review of the algorithms and its applications, in *Proceedings of ICRIC 2019*, edited by P. K. Singh, A. K. Kar, Y. Singh, M. H. Kolekar, and S. Tanwar (Springer International Publishing, Cham, 2020) pp. 47–63.
  - [4] G. A. Tsihrintzis and L. C. Jain, *Machine learning paradigms: advances in deep learning-based technological applications*, Vol. 18 (Springer Nature, 2020).
  - [5] G. Carleo, I. Cirac, K. Cranmer, L. Daudet, M. Schuld, N. Tishby, L. Vogt-Maranto, and L. Zdeborová, Machine learning and the physical sciences, *Reviews of Modern Physics* **91**, 045002 (2019).
  - [6] P. Mehta, M. Bukov, C.-H. Wang, A. G. Day, C. Richardson, C. K. Fisher, and D. J. Schwab, A high-bias, low-variance introduction to machine learning for physicists, *Physics reports* **810**, 1 (2019).
  - [7] Z. Li, J. Yoon, R. Zhang, F. Rajabipour, W. V. Srubar III, I. Dabo, and A. Radlińska, Machine learning in concrete science: applications, challenges, and best practices, *npj Computational Materials* **8**, 1 (2022).
  - [8] S. L. Wu, J. Chan, W. Guan, S. Sun, A. Wang, C. Zhou, M. Livny, F. Carminati, A. Di Meglio, A. C. Li, *et al.*, Application of quantum machine learning using the quantum variational classifier method to high energy physics analysis at the LHC on

- ibm quantum computer simulator and hardware with 10 qubits, *Journal of Physics G: Nuclear and Particle Physics* **48**, 125003 (2021).
- [9] V. Havlíček, A. D. Córcoles, K. Temme, A. W. Harrow, A. Kandala, J. M. Chow, and J. M. Gambetta, Supervised learning with quantum-enhanced feature spaces, *Nature* **567**, 209 (2019).
- [10] M. Schuld and N. Killoran, Quantum machine learning in feature hilbert spaces, *Phys. Rev. Lett.* **122**, 040504 (2019).
- [11] Y. Liu, S. Arunachalam, and K. Temme, A rigorous and robust quantum speed-up in supervised machine learning, *Nature Physics* **17**, 1013 (2021).
- [12] J. A. Keith, V. Vassilev-Galindo, B. Cheng, S. Chmiela, M. Gastegger, K.-R. Müller, and A. Tkatchenko, Combining machine learning and computational chemistry for predictive insights into chemical systems, *arXiv preprint arXiv:2102.06321* (2021).
- [13] M. Sajjan, J. Li, R. Selvarajan, S. H. Sureshbabu, S. S. Kale, R. Gupta, V. Singh, and S. Kais, Quantum machine learning for chemistry and physics, *Chemical Society Reviews* (2022).
- [14] B. Swingle, Unscrambling the physics of out-of-time-order correlators, *Nature Physics* **14**, 988 (2018).
- [15] B. Hall, Matrix lie groups, in *Lie Groups, Lie Algebras, and Representations: An Elementary Introduction* (Springer International Publishing, Cham, 2015) pp. 3–30.
- [16] B. Swingle, G. Bentsen, M. Schleier-Smith, and P. Hayden, Measuring the scrambling of quantum information, *Phys. Rev. A* **94**, 040302 (2016).
- [17] T. Hashizume, G. S. Bentsen, S. Weber, and A. J. Daley, Deterministic fast scrambling with neutral atom arrays, *Phys. Rev. Lett.* **126**, 200603 (2021).
- [18] C.-J. Lin and O. I. Motrunich, Out-of-time-ordered correlators in a quantum ising chain, *Phys. Rev. B* **97**, 144304 (2018).
- [19] S. Pegahan, I. Arakelyan, and J. E. Thomas, Energy-resolved information scrambling in energy-space lattices, *Phys. Rev. Lett.* **126**, 070601 (2021).
- [20] M. Brenes, S. Pappalardi, M. T. Mitchison, J. Goold, and A. Silva, Out-of-time-order correlations and the fine structure of eigenstate thermalization, *Phys. Rev. E* **104**, 034120 (2021).
- [21] R. Fan, P. Zhang, H. Shen, and H. Zhai, Out-of-time-order correlation for many-body localization, *Science Bulletin* **62**, 707 (2017).
- [22] Z.-H. Sun, J. Cui, and H. Fan, Quantum information scrambling in the presence of weak and strong thermalization, *Phys. Rev. A* **104**, 022405 (2021).
- [23] K. K. Sharma and V. P. Gerdt, Quantum information scrambling and entanglement in bipartite quantum states, *Quantum Information Processing* **20**, 1 (2021).
- [24] A. Touil and S. Deffner, Quantum scrambling and the growth of mutual information, *Quantum Science and Technology* **5**, 035005 (2020).
- [25] B. Yan, L. Cincio, and W. H. Zurek, Information scrambling and loschmidt echo, *Phys. Rev. Lett.* **124**, 160603 (2020).
- [26] W. Fu and S. Sachdev, Numerical study of fermion and boson models with infinite-range random interactions, *Phys. Rev. B* **94**, 035135 (2016).
- [27] C. Yin and A. Lucas, Bound on quantum scrambling with all-to-all interactions, *Phys. Rev. A* **102**, 022402 (2020).
- [28] E. Iyoda and T. Sagawa, Scrambling of quantum information in quantum many-body systems, *Phys. Rev. A* **97**, 042330 (2018).
- [29] S. Sachdev, Bekenstein-hawking entropy and strange metals, *Phys. Rev. X* **5**, 041025 (2015).
- [30] X. Mi, P. Roushan, C. Quintana, S. Mandra, J. Marshall, C. Neill, F. Arute, K. Arya, J. Atalaya, R. Babbush, *et al.*, Information scrambling in quantum circuits, *Science* **374**, 1479 (2021).
- [31] Q. Zhu, Z.-H. Sun, M. Gong, F. Chen, Y.-R. Zhang, Y. Wu, Y. Ye, C. Zha, S. Li, S. Guo, H. Qian, H.-L. Huang, J. Yu, H. Deng, H. Rong, J. Lin, Y. Xu, L. Sun, C. Guo, N. Li, F. Liang, C.-Z. Peng, H. Fan, X. Zhu, and J.-W. Pan, Observation of thermalization and information scrambling in a superconducting quantum processor, *Phys. Rev. Lett.* **128**, 160502 (2022).
- [32] M. S. Blok, V. V. Ramasesh, T. Schuster, K. O’Brien, J. M. Kreikebaum, D. Dahlen, A. Morvan, B. Yoshida, N. Y. Yao, and I. Siddiqi, Quantum information scrambling on a superconducting qutrit processor, *Phys. Rev. X* **11**, 021010 (2021).
- [33] K. A. Landsman, C. Figgatt, T. Schuster, N. M. Linke, B. Yoshida, N. Y. Yao, and C. Monroe, Verified quantum information scrambling, *Nature* **567**, 61 (2019).
- [34] J. Harris, B. Yan, and N. A. Sinitsyn, Benchmarking information scrambling, *Phys. Rev. Lett.* **129**, 050602 (2022).
- [35] R. G. Melko, G. Carleo, J. Carrasquilla, and J. I. Cirac, Restricted Boltzmann machines in quantum physics, *Nature Physics* **15**, 887 (2019).
- [36] G. E. Hinton and R. R. Salakhutdinov, Reducing the Dimensionality of Data with Neural Networks, *Science* **313**, 504 (2006).
- [37] G. Torlai and R. G. Melko, Learning thermodynamics with boltzmann machines, *Phys. Rev. B* **94**, 165134 (2016).
- [38] A. Argun, A. Callegari, and G. Volpe, Ising model, in *Simulation of Complex Systems*, 2053-2563 (IOP Publishing, 2021) pp. 2–1 to 2–12.
- [39] S. G. BRUSH, History of the lenz-ising model, *Rev. Mod. Phys.* **39**, 883 (1967).
- [40] G. Torlai, G. Mazzola, J. Carrasquilla, M. Troyer, R. Melko, and G. Carleo, Many-body quantum state tomography with neural networks, *1* (2017), *arXiv:1703.05334*.
- [41] K. Ch’Ng, J. Carrasquilla, R. G. Melko, and E. Khatami, Machine learning phases of strongly correlated fermions, *Physical Review X* **7**, 1 (2017), *arXiv:1609.02552*.
- [42] A. Decelle and C. Furtlehner, Exact training of restricted boltzmann machines on intrinsically low dimensional data, *Phys. Rev. Lett.* **127**, 158303 (2021).
- [43] J. Carrasquilla and R. G. Melko, Machine learning phases of matter, *Nature Physics* **13**, 431 (2017).
- [44] M. Sajjan, S. H. Sureshbabu, and S. Kais, Quantum machine-learning for eigenstate filtration in two-dimensional materials, *J. Am. Chem. Soc.* **10.1021/jacs.1c06246** (2021).
- [45] R. Xia and S. Kais, Quantum machine learning for electronic structure calculations, *Nature communications* **9**, 1 (2018).
- [46] S. Kanno and T. Tada, Many-body calculations for periodic materials via restricted Boltzmann machine-based VQE, *Quantum Science and Technology* **6**, 10.1088/2058-9565/abe139 (2021).
- [47] M. Razavy, *Heisenberg’s Quantum Mechanics* (WORLD SCIENTIFIC, 2011) <https://www.worldscientific.com/doi/pdf/10.1142/7702>.
- [48] K. Hashimoto, K. Murata, and R. Yoshii, Out-of-time-order correlators in quantum mechanics, *Journal of High Energy Physics* **2017**, 10.1007/jhep10(2017)138 (2017).
- [49] H. Shen, P. Zhang, R. Fan, and H. Zhai, Out-of-time-order correlation at a quantum phase transition, *Phys. Rev. B* **96**, 054503 (2017).
- [50] J. Braumuller, A. H. Karamlou, Y. Yanay, B. Kannan, D. K. Kim, M. Kjaergaard, A. Melville, B. M. Niedzielski, Y. Sung, A. Vepsäläinen, R. Winik, J. L. Yoder, T. P. Orlando, S. Gustavsson, C. Tahan, and W. D. Oliver, Probing quantum information propagation with out-of-time-ordered correlators, *Nature Physics* **18**, 172 (2021).
- [51] B. Sundar, A. Elben, L. K. Joshi, and T. V. Zache, Proposal for measuring out-of-time-ordered correlators at finite temperature

- with coupled spin chains, *New Journal of Physics* **24**, 023037 (2022).
- [52] L. D'Alessio, Y. Kafri, A. Polkovnikov, and M. Rigol, From quantum chaos and eigenstate thermalization to statistical mechanics and thermodynamics, *Advances in Physics* **65**, 239 (2016).
- [53] T. Schuster, M. Niu, J. Cotler, T. O'Brien, J. R. McClean, and M. Mohseni, *Learning quantum systems via out-of-time-order correlators* (2022).
- [54] M. A. Nielsen and I. L. Chuang, *Quantum Computation and Quantum Information: 10th Anniversary Edition* (Cambridge University Press, 2010).
- [55] J. Watrous, *The Theory of Quantum Information* (2018).
- [56] A. Globerson, E. Stark, E. Vaadia, and N. Tishby, The minimum information principle and its application to neural code analysis, *Proceedings of the National Academy of Sciences* **106**, 3490 (2009), <https://www.pnas.org/doi/pdf/10.1073/pnas.0806782106>.
- [57] G. De Tomasi, S. Bera, J. H. Bardarson, and F. Pollmann, Quantum mutual information as a probe for many-body localization, *Phys. Rev. Lett.* **118**, 016804 (2017).
- [58] M. M. Wolf, F. Verstraete, M. B. Hastings, and J. I. Cirac, Area laws in quantum systems: Mutual information and correlations, *Phys. Rev. Lett.* **100**, 070502 (2008).
- [59] P. Pfeuty, The one-dimensional ising model with a transverse field, *Annals of Physics* **57**, 79 (1970).
- [60] P. Pfeuty and R. Elliott, The ising model with a transverse field. ii. ground state properties, *Journal of Physics C: Solid State Physics* **4**, 2370 (1971).
- [61] R. Stinchcombe, Ising model in a transverse field. i. basic theory, *Journal of Physics C: Solid State Physics* **6**, 2459 (1973).
- [62] G. Vitagliano, A. Riera, and J. I. Latorre, Volume-law scaling for the entanglement entropy in spin-1/2 chains, *New Journal of Physics* **12**, 113049 (2010).
- [63] D. Sehayek, A. Golubeva, M. S. Albergro, B. Kulchytskyy, G. Torlai, and R. G. Melko, Learnability scaling of quantum states: Restricted boltzmann machines, *Phys. Rev. B* **100**, 195125 (2019).
- [64] R. A. Horn and C. R. Johnson, *Matrix Analysis*, 2nd ed. (Cambridge University Press, 2012).
- [65] T. Koffel, M. Lewenstein, and L. Tagliacozzo, Entanglement entropy for the long-range ising chain in a transverse field, *Physical review letters* **109**, 267203 (2012).
- [66] T. Kuwahara and K. Saito, Area law of noncritical ground states in 1d long-range interacting systems, *Nature communications* **11**, 1 (2020).
- [67] G. Vitagliano, A. Riera, and J. I. Latorre, Volume-law scaling for the entanglement entropy in spin-1/2 chains, *New Journal of Physics* **12**, 113049 (2010).
- [68] Y. Nomura, A. S. Darmawan, Y. Yamaji, and M. Imada, Restricted boltzmann machine learning for solving strongly correlated quantum systems, *Phys. Rev. B* **96**, 205152 (2017).
- [69] K. Choo, A. Mezzacapo, and G. Carleo, Fermionic neural-network states for ab-initio electronic structure, *Nature communications* **11**, 1 (2020).
- [70] S. Lu, X. Gao, and L.-M. Duan, Efficient representation of topologically ordered states with restricted boltzmann machines, *Phys. Rev. B* **99**, 155136 (2019).
- [71] T. Viejira, C. Casert, J. Nys, W. De Neve, J. Haegeman, J. Ryckebusch, and F. Verstraete, Restricted boltzmann machines for quantum states with non-abelian or anyonic symmetries, *Phys. Rev. Lett.* **124**, 097201 (2020).
- [72] C. K. Lee, P. Patil, S. Zhang, and C. Y. Hsieh, Neural-network variational quantum algorithm for simulating many-body dynamics, *Phys. Rev. Research* **3**, 023095 (2021).
- [73] S. H. Sureshbabu, M. Sajjan, S. Oh, and S. Kais, Implementation of quantum machine learning for electronic structure calculations of periodic systems on quantum computing devices, *Journal of Chemical Information and Modeling* (2021).
- [74] P.-J. Yang, M. Sugiyama, K. Tsuda, and T. Yanai, Artificial neural networks applied as molecular wave function solvers, *Journal of Chemical Theory and Computation* **16**, 3513 (2020).
- [75] C. Ciliberto, M. Herbster, A. D. Ialongo, M. Pontil, A. Rocchetto, S. Severini, and L. Wossnig, Quantum machine learning: a classical perspective, *Proceedings of the Royal Society A: Mathematical, Physical and Engineering Sciences* **474**, 20170551 (2018).
- [76] N. Le Roux and Y. Bengio, Representational Power of Restricted Boltzmann Machines and Deep Belief Networks, *Neural Computation* **20**, 1631 (2008).
- [77] D.-L. Deng, X. Li, and S. Das Sarma, Quantum entanglement in neural network states, *Phys. Rev. X* **7**, 021021 (2017).
- [78] P. M. Long and R. A. Servedio, Restricted Boltzmann Machines are hard to approximately evaluate or simulate, *ICML 2010 - Proceedings, 27th International Conference on Machine Learning*, 703 (2010).
- [79] C. Bellinger, R. Coles, M. Crowley, and I. Tambllyn, Reinforcement learning in a physics-inspired semi-markov environment (2020), [arXiv:2004.07333 \[cs.LG\]](https://arxiv.org/abs/2004.07333).
- [80] F. Musil, A. Grisafi, A. P. Bartók, C. Ortner, G. Csányi, and M. Ceriotti, Physics-inspired structural representations for molecules and materials, *Chemical Reviews* **121**, 9759 (2021).
- [81] G. E. Karniadakis, I. G. Kevrekidis, L. Lu, P. Perdikaris, S. Wang, and L. Yang, Physics-informed machine learning, *Nature Reviews Physics* **3**, 422 (2021).

### Appendix A: Invariants of motion-Proof of Theorem 1 in main manuscript

We are now in a position to prove the assertions of Theorem 1 in the main manuscript  $\forall \alpha, \beta \in \{x, y\}$

1) For Theorem 1 (1), See Appendix E (Lemma E.3)

#### 2) Real part

For the real part of  $C_{\sigma^\alpha, \sigma^\beta}(0, 0, \vec{X}, \tau)$  we substitute in Theorem 1(a)

$$\xi_{\sigma^\alpha, \sigma^\beta}(\vec{X}, \tau) = \text{Re}(C_{\sigma^\alpha, \sigma^\beta}(0, 0, \vec{X}, \tau)) = C_{r, \sigma^\alpha, \sigma^\beta}(0, 0, \vec{X}, \tau) \quad (\text{A1})$$

Thus we have to show

$$\text{a) } \underline{-2\dot{C}_{r, \sigma^\alpha, \sigma^\beta}(0, 0, \vec{X}, \tau) \cos(\tau) - 2C_{r, \sigma^\alpha, \sigma^\beta}(0, 0, \vec{X}, \tau) \sin(\tau)}$$

*Proof.*

Let's call the expression above as  $I_{r1}$ . Using the definition of  $C_{r, \sigma^\alpha, \sigma^\beta}(0, 0, \vec{X}, \tau)$  as

$$C_{r, \sigma^\alpha, \sigma^\beta}(0, 0, \vec{X}, \tau) = \langle I_{2 \times 2} - \frac{1}{2} \hat{\Theta}_{\alpha, \beta}^\dagger(\tau) \hat{\Theta}_{\alpha, \beta}(\tau) \rangle_{\rho_{th}} \quad (\text{A2})$$

where  $\hat{\Theta}_{\alpha, \beta}(t) = [\sigma^\alpha(v_k, 0), \sigma^\beta(h_m, t)]$  (see Lemma D.2) one can show the following

$$\begin{aligned} I_{r1} &= \left\langle \frac{\partial^2 \hat{\Theta}_{\alpha, \beta}^\dagger(\tau) \hat{\Theta}_{\alpha, \beta}(\tau)}{\partial \tau^2} \cos(\tau) + \frac{\partial \hat{\Theta}_{\alpha, \beta}^\dagger(\tau) \hat{\Theta}_{\alpha, \beta}(\tau)}{\partial \tau} \sin(\tau) - \frac{\partial \hat{\Theta}_{\alpha, \beta}^\dagger(\tau) \hat{\Theta}_{\alpha, \beta}(\tau)}{\partial t} \sin(\tau) - 2(I_{2 \times 2} - \frac{1}{2} \hat{\Theta}_{\alpha, \beta}^\dagger(\tau) \hat{\Theta}_{\alpha, \beta}(\tau)) \cos(\tau) \right\rangle_{\rho_{th}} \\ &= \left\langle \frac{\partial^2 \hat{\Theta}_{\alpha, \beta}^\dagger(\tau) \hat{\Theta}_{\alpha, \beta}(\tau)}{\partial \tau^2} \cos(\tau) - 2(I_{2 \times 2} - \frac{1}{2} \hat{\Theta}_{\alpha, \beta}^\dagger(t) \hat{\Theta}_{\alpha, \beta}(\tau)) \cos(\tau) \right\rangle_{\rho_{th}} \\ &= 2 \left\langle \frac{1}{2} \frac{\partial^2 \hat{\Theta}_{\alpha, \beta}^\dagger(\tau) \hat{\Theta}_{\alpha, \beta}(\tau)}{\partial \tau^2} - (I_{2 \times 2} - \frac{1}{2} \hat{\Theta}_{\alpha, \beta}^\dagger(t) \hat{\Theta}_{\alpha, \beta}(\tau)) \right\rangle_{\rho_{th}} \cos(\tau) \\ &= \frac{2}{(4W_m^k)^2} \left\langle \frac{1}{2} \frac{\partial^2 \hat{\Theta}_{\alpha, \beta}^\dagger(t) \hat{\Theta}_{\alpha, \beta}(t)}{\partial t^2} - (4W_m^k)^2 (I_{2 \times 2} - \frac{1}{2} \hat{\Theta}_{\alpha, \beta}^\dagger(t) \hat{\Theta}_{\alpha, \beta}(t)) \right\rangle_{\rho_{th}} \cos(4W_m^k t) \quad \because \tau = 4W_m^k t \\ &= 0 \quad \because \text{Lemma D.3(1)} \quad \forall \alpha, \beta \in \{x, y\} \end{aligned}$$

□

$$\text{b) For this one we have to show } \underline{-2\dot{C}_{r, \sigma^\alpha, \sigma^\beta}(0, 0, \vec{X}, \tau) \sin(\tau) + 2C_{r, \sigma^\alpha, \sigma^\beta}(0, 0, \vec{X}, \tau) \cos(\tau)}$$

*Proof.*

Let the expression in Eq. b) be called  $I_{r2}$ . Similar to Eq.a), Eq.b) can either be verified explicitly or by noting  $I_{r2} = I_{r1}(\tau \rightarrow \tau - \frac{\pi}{2})$ . The invariance of  $I_{r2}$  thereafter follows from the invariance of  $I_{r1}$  proven in a) above □



### Imag part

For the imaginary part of  $C_{\sigma^\alpha, \sigma^\beta}(0, 0, \vec{X}, \tau)$  we substitute in Theorem 1(a)

$$\xi_{\sigma^\alpha, \sigma^\beta}(\vec{X}, \tau) = \text{Im}(C_{\sigma^\alpha, \sigma^\beta}(0, 0, \vec{X}, \tau)) = C_{i, \sigma^\alpha, \sigma^\beta}(0, 0, \vec{X}, \tau) \quad (\text{A3})$$

Thus we have to show

$$\text{a) } \underline{-2\dot{C}_{i, \sigma^\alpha, \sigma^\beta}(0, 0, \vec{X}, \tau) \cos(\tau) - 2C_{i, \sigma^\alpha, \sigma^\beta}(0, 0, \vec{X}, \tau) \sin(\tau)}$$

*Proof.* Let's call the expression above as  $I_{i1}$ . Using the definition of  $C_{i, \sigma^\alpha, \sigma^\beta}(0, 0, \vec{X}, \tau)$  as

$$C_{i, \sigma^\alpha, \sigma^\beta}(0, 0, \vec{X}, \tau) = -\frac{i}{2} \langle \hat{\Phi}_{\alpha, \beta}^\dagger(t) \hat{\Theta}_{\alpha, \beta}(\tau) \rangle_{\rho_{th}} \quad (\text{A4})$$

where  $\hat{\Phi}_{\alpha, \beta}(t) = \{\sigma^\alpha(v_k, 0), \sigma^\beta(h_m, t)\}_+$  (see Lemma D.2), one can show the following

$$\begin{aligned} I_{i1} &= i \left\langle \frac{\partial^2 \hat{\Phi}_{\alpha, \beta}^\dagger(\tau) \hat{\Theta}_{\alpha, \beta}(\tau)}{\partial \tau^2} \cos(\tau) - \frac{\partial \hat{\Phi}_{\alpha, \beta}^\dagger(\tau) \hat{\Theta}_{\alpha, \beta}(\tau)}{\partial \tau} \sin(\tau) + \frac{\partial \hat{\Phi}_{\alpha, \beta}^\dagger(\tau) \hat{\Theta}_{\alpha, \beta}(\tau)}{\partial \tau} \sin(\tau) + \hat{\Phi}_{\alpha, \beta}^\dagger(\tau) \hat{\Theta}_{\alpha, \beta}(\tau) \cos(\tau) \right\rangle_{\rho_{th}} \quad \square \\ &= i \left\langle \frac{\partial^2 \hat{\Phi}_{\alpha, \beta}^\dagger(\tau) \hat{\Theta}_{\alpha, \beta}(\tau)}{\partial \tau^2} \cos(\tau) + \hat{\Phi}_{\alpha, \beta}^\dagger(\tau) \hat{\Theta}_{\alpha, \beta}(\tau) \cos(\tau) \right\rangle_{\rho_{th}} \\ &= \frac{i}{(4W_m^k)^2} \left\langle \frac{\partial^2 \hat{\Phi}_{\alpha, \beta}^\dagger(t) \hat{\Theta}_{\alpha, \beta}(t)}{\partial t^2} \cos(4W_m^k t) + (4W_m^k)^2 \hat{\Phi}_{\alpha, \beta}^\dagger(t) \hat{\Theta}_{\alpha, \beta}(t) \cos(4W_m^k t) \right\rangle_{\rho_{th}} \quad \because \tau = 4W_m^k t \\ &= 0 \quad \because \text{Lemma D.3(2)} \quad \forall \alpha, \beta \in \{x, y\} \end{aligned}$$

$$\text{b) For this one we have to show } \underline{-2\dot{C}_{i, \sigma^\alpha, \sigma^\beta}(0, 0, \vec{X}, \tau) \sin(\tau) + 2C_{i, \sigma^\alpha, \sigma^\beta}(0, 0, \vec{X}, \tau) \cos(\tau)}$$

*Proof.*

Let the expression in Eq. b) be called  $I_{i2}$ . Similar to Eq.a), Eq.b) can either be verified explicitly or by noting  $I_{i2} = I_{i1}(\tau \rightarrow \tau - \frac{\pi}{2})$ . The invariance of  $I_{i2}$  thereafter follows from the invariance of  $I_{i1}$  proven in a) above  $\square$

Using the definitions for  $\Theta_{\alpha,\beta,\tau} = [\sigma^\alpha(v_k, 0), \sigma^\beta(h_m, t)]$  and  $\Phi_{\alpha,\beta,\tau} = \{\sigma^\alpha(v_k, 0), \sigma^\beta(h_m, t)\}_+$  as given in Lemma D.2, one can enlist the initial conditions satisfied by  $C_{r\sigma^\alpha,\sigma^\beta}(0, 0, \vec{X}, \tau)$  and  $C_{i\sigma^\alpha,\sigma^\beta}(0, 0, \vec{X}, \tau)$  as follows:

$$C_{r\sigma^\alpha,\sigma^\beta}(0, 0, \vec{X}, 0) = \langle I_{2 \times 2} - \frac{1}{2} \hat{\Theta}_{\alpha,\beta}^\dagger(0) \hat{\Theta}_{\alpha,\beta}(0) \rangle_{\rho_{th}} = 1 \quad (A5)$$

$$(\because \hat{\Theta}_{\alpha,\beta}(0) = 0)$$

$$\dot{C}_{r\sigma^\alpha,\sigma^\beta}(0, 0, \vec{X}, 0) = -\frac{1}{2} \langle \frac{\partial}{\partial \tau} \hat{\Theta}_{\alpha,\beta}^\dagger(\tau) \hat{\Theta}_{\alpha,\beta}(\tau) \rangle_{\rho_{th}}|_0 = 0 \quad (A6)$$

$$(\because \hat{\Theta}_{\alpha,\beta}(0) = \hat{\Theta}_{\alpha,\beta}^\dagger(0) = 0)$$

$$C_{i\sigma^\alpha,\sigma^\beta}(0, 0, \vec{X}, 0) = -\frac{i}{2} \langle \hat{\Phi}_{\alpha,\beta}^\dagger(0) \hat{\Theta}_{\alpha,\beta}(0) \rangle_{\rho_{th}} = 0 \quad (A7)$$

$$(\because \hat{\Theta}_{\alpha,\beta}(0) = 0)$$

$$\begin{aligned} \dot{C}_{i\sigma^\alpha,\sigma^\beta}(0, 0, \vec{X}, 0) &= -\frac{i}{2} \langle \frac{\partial}{\partial \tau} \hat{\Phi}_{\alpha,\beta}^\dagger(\tau) \hat{\Theta}_{\alpha,\beta}(\tau) \rangle_{\rho_{th}}|_0 \\ &= \langle \frac{\partial}{\partial \tau} \sigma^z(v_k, 0) \sigma^z(h_m, 0) \sin(4W_m^k t) \rangle_{\rho_{th}} \\ &= \langle \sigma^z(v_k, 0) \sigma^z(h_m, 0) \rangle_{\rho_{th}} \\ &(\text{ see Lemma D.2(2) }) \end{aligned} \quad (A8)$$

Using Eq.A5, A6, A7, A8 one can establish the following corollary to Theorem 1 in the main manuscript

**Corollary A.0.1.** *The following statements are true*

- $C_{r\sigma^\alpha,\sigma^\beta}(0, 0, \vec{X}, \tau) = \cos(4W_m^k t)$

*Proof.*

$$\begin{aligned} C_{r\sigma^\alpha,\sigma^\beta}(0, 0, \vec{X}, \tau) &= \frac{I_{r1}}{2} \cos(\tau) + i \frac{I_{r2}}{2} \sin(\tau) \quad (\because \text{Eq.(a)} \times \sin(\tau) - \text{Eq.(b)} \times \cos(\tau)) \\ &= \cos(\tau) \quad (\text{see Eq.A5, A6}) \\ &= \cos(4W_m^k t) \quad \because \tau = 4W_m^k t \end{aligned} \quad \square$$

- $C_{i\sigma^\alpha,\sigma^\beta}(0, 0, \vec{X}, \tau) = \langle \sigma^z(v_k, 0) \sigma^z(h_m, 0) \rangle \sin(4W_m^k t)$

*Proof.*

$$\begin{aligned} C_{i\sigma^\alpha,\sigma^\beta}(0, 0, \vec{X}, \tau) &= \frac{I_{i1}}{2} \cos(\tau) + i \frac{I_{i2}}{2} \sin(\tau) \quad (\because \text{Eq.(a)} \times \sin(\tau) - \text{Eq.(b)} \times \cos(\tau)) \\ &= \langle \sigma^z(v_k, 0) \sigma^z(h_m, 0) \rangle \sin(\tau) \quad (\text{see Eq.A7, A8}) \\ &= \langle \sigma^z(v_k, 0) \sigma^z(h_m, 0) \rangle \sin(4W_m^k t) \quad (\because \tau = 4W_m^k t) \end{aligned} \quad \square$$

**Corollary A.0.2.** *In addition to the above invariants, following are also the invariants of motion for  $C_{r\sigma^\alpha,\sigma^\beta}(0, 0, \vec{X}, \tau)$  and  $C_{i\sigma^\alpha,\sigma^\beta}(0, 0, \vec{X}, \tau)$*

- $(\dot{C}_{r\sigma^\alpha,\sigma^\beta}(0, 0, \vec{X}, \tau)^2 - C_{r\sigma^\alpha,\sigma^\beta}(0, 0, \vec{X}, \tau)^2) \sin(2\tau) - 2\dot{C}_{r\sigma^\alpha,\sigma^\beta}(0, 0, \vec{X}, \tau) C_{r\sigma^\alpha,\sigma^\beta}(0, 0, \vec{X}, \tau) \cos(2\tau)$

*Proof.*

Can be verified through explicit evaluation using the solution  $C_{r\sigma^\alpha,\sigma^\beta}(0, 0, \vec{X}, \tau)$  in Corollary A.0.1, or by combining the invariants  $I_{r1}, I_{r1}$  in Eq.a) and Eq.b) as  $\frac{1}{2} I_{r1} I_{r2}$ . This invariant is plotted in Fig.2(a)  $\square$

- $(\dot{C}_{r\sigma^\alpha,\sigma^\beta}(0, 0, \vec{X}, \tau)^2 + C_{r\sigma^\alpha,\sigma^\beta}(0, 0, \vec{X}, \tau)^2)$

*Proof.*

Can be verified through explicit evaluation using the solution  $C_{r\sigma^\alpha, \sigma^\beta}(0, 0, \vec{X}, \tau)$  in Corollary A.0.1, or by combining the invariants  $I_{r1}, I_{r1}$  in Eq.a) and Eq.b) as  $\frac{1}{4}(I_{r1}^2 + I_{r2}^2)$   $\square$

Exactly similar invariants can be obtained for  $C_{r\sigma^\alpha, \sigma^\beta}(0, 0, \vec{X}, \tau)$  by substituting  $C_{r\sigma^\alpha, \sigma^\beta}(0, 0, \vec{X}, \tau) \rightarrow C_{i\sigma^\alpha, \sigma^\beta}(0, 0, \vec{X}, \tau)$  in the above expressions.

It is possible to define generators associated with these invariants which possess an underlying Lie Algebraic structure. The ramifications of such generators on the full phase-space of the OTOC strings will be explored in the future. We thus see that instead of a direct evaluation of the OTOC, evaluation through the invariants described in Theorem 1 of the main manuscript offers a fuller characterization of the phase space with richer insight into the geometry of the manifold.

## Appendix B: Relationship between $\eta(\vec{X})$ (see Eq.9) and $\mathcal{I}(v_k, h_m)$ - Proof of Theorem 2 in main manuscript

Using the thermal state in Eq.4, the eigenvalues of the two-particle density matrix for the learner  $G$  can be readily computed as

$$\lambda_1(^2\rho(v_k, h_m)) = \frac{e^{-a_k - \sum_{j \neq m} W_j^k f^z(h_j)} e^{-b_m - \sum_{i \neq k} W_m^i f^z(v_i)} e^{-W_m^k}}{\tilde{Z}(v_k, h_m)} \quad (B1)$$

$$\lambda_2(^2\rho(v_k, h_m)) = \frac{e^{a_k + \sum_{j \neq m} W_j^k f^z(h_j)} e^{b_m + \sum_{i \neq k} W_m^i f^z(v_i)} e^{-W_m^k}}{\tilde{Z}(v_k, h_m)} \quad (B2)$$

$$\lambda_3(^2\rho(v_k, h_m)) = \frac{e^{-a_k - \sum_{j \neq m} W_j^k f^z(h_j)} e^{b_m + \sum_{i \neq k} W_m^i f^z(v_i)} e^{W_m^k}}{\tilde{Z}(v_k, h_m)} \quad (B3)$$

$$\lambda_4(^2\rho(v_k, h_m)) = \frac{e^{a_k + \sum_{j \neq m} W_j^k f^z(h_j)} e^{-b_m - \sum_{i \neq k} W_m^i f^z(v_i)} e^{W_m^k}}{\tilde{Z}(v_k, h_m)} \quad (B4)$$

where  $f^z(v_k)/f^z(h_m) \in \{+1, -1\}$  are eigenvalues of  $\sigma^z(v_k, 0)/\sigma^z(h_m, 0)$  respectively  $\forall \{k, m\}$ . Also  $\tilde{Z}(v_k, h_m)$  is defined as

$$\tilde{Z}(v_k, h_m) = \sum_{f^z(v_k), f^z(h_m)} e^{-a_k f^z(v_k) - \sum_{j \neq m} W_j^k f^z(v_k) f^z(h_j)} e^{-b_m f^z(h_m)} e^{-\sum_{i \neq k} W_m^i f^z(v_i) f^z(h_m)} e^{-W_m^k f^z(v_k) f^z(h_m)} \quad (B5)$$

The corresponding eigenvectors are  $|0(v_k)0(h_m)\rangle$ ,  $|1(v_k)1(h_m)\rangle$ ,  $|0(v_k)1(h_m)\rangle$  and  $|1(v_k)0(h_m)\rangle$  respectively. The eigenvalues for one-particle density matrix  $^1\rho(\xi_i, 0)$  for a neuron  $\xi_i$  in the learner  $G$ , by contraction from Eq.B1, B2, B3, B4 are

$$\begin{aligned} \lambda_1(^1\rho(\xi_i)) &= \lambda_i(^2\rho(v_k, h_m)) + \lambda_j(^2\rho(v_k, h_m)) \\ &\quad (\text{if } \xi_i = v_k, (i, j) = (1, 3)) \\ &\quad (\text{if } \xi_i = h_m, (i, j) = (1, 4)) \\ &= \frac{1}{2} + \langle \sigma^z(\xi_i) \rangle_{\rho_{th}(\vec{X}, \vec{v}, \vec{h})} \end{aligned} \quad (B6)$$

$$\begin{aligned} \lambda_2(^1\rho(\xi_i)) &= \lambda_i(^2\rho(v_k, h_m)) + \lambda_j(^2\rho(v_k, h_m)) \\ &\quad (\text{if } \xi_i = v_k, (i, j) = (2, 4)) \\ &\quad (\text{if } \xi_i = h_m, (i, j) = (2, 3)) \\ &= \frac{1}{2} - \langle \sigma^z(\xi_i) \rangle_{\rho_{th}(\vec{X}, \vec{v}, \vec{h})} \end{aligned} \quad (B7)$$

with respective eigenvectors as  $|0(\xi_i)\rangle$  and  $|1(\xi_i)\rangle$  where  $\xi_i \in (v_k, h_m)$  and  $\sigma^z(\xi_i, 0)$  is

$$\langle \sigma^z(\xi_i) \rangle_{\rho_{th}(\vec{X}, \vec{v}, \vec{h})} = \begin{cases} \tanh(-a_k - \sum_j W_j^k f^z(h_j, 0)), \\ \quad (\text{if } \xi_i = v_k) \\ \tanh(-b_m - \sum_i W_m^i f^z(v_i, 0)), \\ \quad (\text{if } \xi_i = h_m) \end{cases} \quad (B8)$$

Now using these information, one can deduce expressions for  $S(^2\rho(v_k, h_m))$  and  $S(^1\rho(v_k))$ ,  $S(^1\rho(h_m))$  and hence of  $\mathcal{I}(v_k, h_m)$  as follows

$$\begin{aligned}
\mathcal{I}(v_k, h_m) &= S(^1\rho(v_k)) + S(^1\rho(h_m)) - S(^2\rho(v_k, h_m)) \\
&= -\lambda_1(^1\rho(v_k))\log_2(\lambda_1(^1\rho(v_k))) - \lambda_2(^1\rho(v_k))\log_2(\lambda_2(^1\rho(v_k))) - \lambda_1(^1\rho(h_m))\log_2(\lambda_1(^1\rho(h_m))) \\
&\quad - \lambda_2(^1\rho(h_m))\log_2(\lambda_2(^1\rho(h_m))) + \lambda_1(^2\rho(v_k, h_m))\log_2(\lambda_1(^2\rho(v_k, h_m))) + \lambda_2(^2\rho(v_k, h_m))\log_2(\lambda_2(^2\rho(v_k, h_m))) \\
&\quad + \lambda_3(^2\rho(v_k, h_m))\log_2(\lambda_3(^2\rho(v_k, h_m))) + \lambda_4(^2\rho(v_k, h_m))\log_2(\lambda_4(^2\rho(v_k, h_m))) \\
&\quad - (\lambda_1(^2\rho(v_k, h_m)) + \lambda_3(^2\rho(v_k, h_m))\log_2(\lambda_1(^2\rho(v_k, h_m)) + \lambda_3(^2\rho(v_k, h_m))) \\
&\quad - (\lambda_2(^2\rho(v_k, h_m)) + \lambda_4(^2\rho(v_k, h_m))\log_2(\lambda_2(^2\rho(v_k, h_m)) + \lambda_4(^2\rho(v_k, h_m))) \\
&\quad - (\lambda_1(^2\rho(v_k, h_m)) + \lambda_4(^2\rho(v_k, h_m))\log_2(\lambda_1(^2\rho(v_k, h_m)) + \lambda_4(^2\rho(v_k, h_m))) \\
&\quad - (\lambda_2(^2\rho(v_k, h_m)) + \lambda_3(^2\rho(v_k, h_m))\log_2(\lambda_2(^2\rho(v_k, h_m)) + \lambda_3(^2\rho(v_k, h_m))) \\
&\quad + \lambda_1(^2\rho(v_k, h_m))\log_2(\lambda_1(^2\rho(v_k, h_m))) + \lambda_2(^2\rho(v_k, h_m))\log_2(\lambda_2(^2\rho(v_k, h_m))) \\
&\quad + \lambda_3(^2\rho(v_k, h_m))\log_2(\lambda_3(^2\rho(v_k, h_m))) + \lambda_4(^2\rho(v_k, h_m))\log_2(\lambda_4(^2\rho(v_k, h_m)))
\end{aligned} \tag{B9}$$

wherein in the last equality in Eq.B9, contraction schemes from Eq.B6,B7 were used. Eq.B9 thus expresses  $\mathcal{I}(v_k, h_m)$  in terms of the eigenvalues of  $^2\rho(v_k, h_m)$ . Apart from this the normalization condition also inter-relates the eigenvalues as

$$\lambda_1(^2\rho(v_k, h_m)) + \lambda_2(^2\rho(v_k, h_m)) + \lambda_3(^2\rho(v_k, h_m)) + \lambda_4(^2\rho(v_k, h_m)) = 1 \tag{B10}$$

The expression for the  $\eta(\vec{X})$  as follows

$$\begin{aligned}
\eta(\vec{X}) &= \text{Cov}(\sigma^x(v_k, 0), \sigma^x(h_m, 0)) \\
&= \text{Tr}(\sigma^x(v_k, 0)\sigma^x(h_m, 0) ^2\rho(v_k, h_m)) - \langle \sigma^z(v_k, 0) \rangle_{\rho_{v_k}} \langle \sigma^z(h_m, 0) \rangle_{\rho_{h_m}} \\
&= \lambda_1(^2\rho(v_k, h_m)) + \lambda_2(^2\rho(v_k, h_m)) - \lambda_3(^2\rho(v_k, h_m)) - \left( \sum_{i=1,3} \lambda_i(^2\rho(v_k, h_m)) - \sum_{i=2,4} \lambda_i(^2\rho(v_k, h_m)) \right) \\
&\quad \left( \sum_{i=1,4} \lambda_i(^2\rho(v_k, h_m)) - \sum_{i=2,3} \lambda_i(^2\rho(v_k, h_m)) \right)
\end{aligned} \tag{B11}$$

Also to ensure positive-semi-definiteness of  $^2\rho(v_k, h_m)$ , we have

$$\lambda_i(^2\rho(v_k, h_m)) \geq 0 \quad \forall i \in \{1, 2, 3, 4\} \tag{B12}$$

Thus we see that Eq.B9 combined with B10, Eq.B12 for a given value of  $\eta(\vec{X})$  in Eq.B11 completely defines the  $\mathcal{I} - \eta$  space in terms of the spectrum of  $^2\rho(v_k, h_m)$

#### Lower Bound(LB)

The minimization of Eq.B9 over the spectrum of  $^2\rho(v_k, h_m)$  with the constraints defined in Eq.B10, Eq.B12 and Eq.B11(for a fixed value of  $\eta(\vec{X})$ ) gives the following condition

$$\begin{aligned}
\lambda_1(^2\rho(v_k, h_m)) &= \lambda_2(^2\rho(v_k, h_m)) = \lambda_a(\text{say}) \\
\lambda_3(^2\rho(v_k, h_m)) &= \lambda_4(^2\rho(v_k, h_m)) = \lambda_b(\text{say})
\end{aligned} \tag{B13}$$

Substituting the above conditions in Eq.B10 and in Eq.B9 leads to the following

$$\lambda_b = \frac{1}{2} - \lambda_a \tag{B14}$$

$$\eta(\vec{X}) = 4\lambda_a - 1 \quad (\because \text{Eq. B14}) \tag{B15}$$



Substituting Eq.B15, B14 and the conditions in Eq.B13, in Eq.B9 yields the lower bound  $LB$  as

$$\begin{aligned}
LB &= \mathcal{I}_{LB}(v_k, h_m) = 2 + 2\lambda_a \log_2(\lambda_a) + 2\lambda_b \log_2(\lambda_b) \\
&= 2 + 2\lambda_a \log_2(\lambda_a) + 2\left(\frac{1}{2} - \lambda_a\right) \log_2\left(\frac{1}{2} - \lambda_a\right) \\
&= 2 + 2\lambda_a \log_2(\lambda_a) + (1 - 2\lambda_a) \log_2\left(\frac{1}{2} - \lambda_a\right) \\
&= 2 + \left(\frac{\eta(\vec{X}) + 1}{2}\right) \log_2\left(\frac{\eta(\vec{X}) + 1}{4}\right) \\
&\quad + \left(\frac{1 - \eta(\vec{X})}{2}\right) \log_2\left(\frac{1 - \eta(\vec{X})}{4}\right) \quad \because \text{Eq.B15}
\end{aligned} \tag{B16}$$

Note that  $LB$  is symmetric about  $\eta(\vec{X}) = 0$  and remains unchanged on substitution of  $\eta(\vec{X}) \rightarrow -\eta(\vec{X})$ . Also,  $LB$  is mathematically only defined if  $-1 \leq \eta(\vec{X}) \leq 1$  which is true for covariances of Pauli operators in the learner  $G$  (a direct by-product of Cauchy-Schwartz inequality and idempotency of Pauli operators which bounds their respective variances to within 1).

#### Upper Bound(UB)

The maximization of Eq.B9 over the spectrum of  $^2\rho(v_k, h_m)$  with the constraints defined in Eq.B10, Eq.B12 and Eq.B11 (for a fixed value of  $\eta(\vec{X})$ ) gives the following condition

$$\begin{aligned}
\lambda_1(^2\rho(v_k, h_m)) &= \lambda_2(^2\rho(v_k, h_m)) = 0 \\
\lambda_3(^2\rho(v_k, h_m)) &= \lambda_a(\text{say}) \\
\lambda_4(^2\rho(v_k, h_m)) &= \lambda_b(\text{say})
\end{aligned} \tag{B17}$$

Now using Eq.B17 in Eq.B10 and Eq.B11 we get

$$\begin{aligned}
\lambda_b &= 1 - \lambda_a \\
\eta(\vec{X}) &= -1 + (2\lambda_a - 1)^2 \\
&= 4\lambda_a(4\lambda_a - 1) \quad (\because \text{Eq.B18}) \\
\lambda_a &= \frac{1 \pm \sqrt{1 + (-1)^\gamma \eta(\vec{X})}}{2}
\end{aligned} \tag{B19}$$

wherein in the last equality to maintain positive semi-definiteness of  $\lambda_a$  (hence for  $\lambda_3$ ) in both the roots, a factor of  $(-1)^\gamma$  was used along with the condition  $-1 \leq \eta(\vec{X}) \leq 1$ . Note that  $\gamma = 0$  when  $\eta(\vec{X}) < 0$  and  $\gamma = 1$  when  $\eta(\vec{X}) \geq 0$ . Now substituting Eq.B17, Eq.B18 and Eq.B19 in Eq.B9 we obtain UB as

$$\begin{aligned}
UB &= \mathcal{I}_{UB}(v_k, h_m) \\
&= -\lambda_a \log_2(\lambda_a) - \lambda_b \log_2(\lambda_b) \\
&= -\lambda_a \log_2(\lambda_a) - (1 - \lambda_a) \log_2(1 - \lambda_a) \quad (\because \text{Eq.B18}) \\
&= \left(\frac{1}{2} + \frac{\sqrt{1 + (-1)^\gamma \eta(\vec{X})}}{2}\right) \log_2\left(\frac{1}{2} + \frac{\sqrt{1 + (-1)^\gamma \eta(\vec{X})}}{2}\right) \\
&\quad - \left(\frac{1}{2} - \frac{\sqrt{1 + (-1)^\gamma \eta(\vec{X})}}{2}\right) \log_2\left(\frac{1}{2} - \frac{\sqrt{1 + (-1)^\gamma \eta(\vec{X})}}{2}\right) \\
&\quad (\because \text{Eq.B19})
\end{aligned} \tag{B20}$$

where substitution of either root from Eq.B19 would lead to the same  $UB$  due to symmetry

#### Appendix C: General formulation for OTOC

As indicated in the text, every OTOC comprises two unitary operators  $U_1(0), U_2(0)$  chosen usually at two non-local sites (here  $\{1, 2\}$  for instance) within a system. The rate at which the information propagates through the system in real-time is

thereafter quantified using the  $C_{U_1, U_2}(t) = \langle U_1^\dagger(0)U_2^\dagger(t)U_1(0)U_2(t) \rangle$ , For measurement purposes, the  $Re(C_{U_1, U_2}(t))$  is often related in literature to the commutator product given as  $\langle [U_1(0), U_2(t)]^\dagger [U_1(0), U_2(t)] \rangle$  where by virtue of construction of the observable, positive semi-definiteness is ensured. The origin of such a choice is attributed to studying chaotic classical systems wherein an analogous expression for Poisson bracket  $\{x(0), p(t)\}_{P_B}$  is used to probe sensitivity to initial conditions. Since in our work we show that the imaginary part  $Im(C_{U_1, U_2}(t))$  can also be informative about correlation content within the sub-units of the learner  $G$ , we offer herein a general formulation for OTOCs of arbitrary systems using newly constructed positive semi-definite operators involving not only commutators ( $[\cdot]$ ) as above but anti-commutators ( $\{\cdot\}_+$ ). The advantage of the formulation is the offered generality in the theory of OTOCs in the quantum domain and also the flexibility in projecting both the real and imaginary component of  $C_{U_1, U_2}(t)$  based on user-defined preferences while still maintaining positive semi-definiteness of the observables probed. To this end, let us define a probe as

$$L_{U_1, U_2}(\lambda_1, \lambda_2, t) = \lambda_1 A(U_1, U_2, t) + i\lambda_2 B(U_1, U_2, t) \quad (C1)$$

$$A(U_1, U_2, t) = \{U_1(0), U_2(t)\}_+ \quad (C2)$$

$$B(U_1, U_2, t) = [U_1(0), U_2(t)] \quad (C3)$$

$$\lambda_1, \lambda_2 \in \mathcal{R} \quad (C4)$$

Using Eq.C1 and the definition for  $C_{U_1, U_2}(0, 0, 1, 1, t)$ , it is easy to show

$$\begin{aligned} Re(C_{U_1, U_2}(0, 0, 1, 1, t)) &= Re(\langle U_1^\dagger(0)U_2^\dagger(t)U_1(0)U_2(t) \rangle) \\ &= 1 - \frac{\langle B(U_1, U_2, t)^\dagger B(U_1, U_2, t) \rangle}{2} \quad \because \text{Eq. C3} \\ &= 1 - \frac{\langle L_{U_1, U_2}(0, 1, t)^\dagger L_{U_1, U_2}(0, 1, t) \rangle}{2} \quad \because \text{Eq. C1} \end{aligned} \quad (C5)$$

and

$$\begin{aligned} Im(C_{U_1, U_2}(t)) &= Im(\langle U_1^\dagger(0)U_2^\dagger(t)U_1(0)U_2(t) \rangle) \\ &= -\frac{1}{2} \langle (A(U_1, U_2, t)^\dagger iB(U_1, U_2, t)) \rangle \quad \because \text{Eq. C2, C3} \\ &= \frac{1}{4} \langle L_{U_1, U_2}(0, 1, t)^\dagger L_{U_1, U_2}(0, 1, t) \rangle + \frac{1}{4} \langle L_{U_1, U_2}(1, 0, t)^\dagger L_{U_1, U_2}(1, 0, t) \rangle \\ &\quad - \frac{1}{4} \langle L_{U_1, U_2}(1, 1, t)^\dagger L_{U_1, U_2}(1, 1, t) \rangle \quad \because \text{Eq. C1} \end{aligned} \quad (C6)$$

Note that all combinations of  $L_{U_1, U_2}(\lambda_1, \lambda_2, t)^\dagger L_{U_1, U_2}(\lambda_1, \lambda_2, t)$  are positive semi-definite by construction and hence is used in the same vein as the usual commutators for OTOCs are traditionally defined but nonetheless offers a much more general framework for investigating the operator string  $C_{U_1, U_2}(t)$

**Appendix D: Time dependence of  $\{\sigma^\alpha(v_k, 0), \sigma^\beta(h_m, t)\}_+$  and  $[\sigma^\alpha(v_k, 0), \sigma^\beta(h_m, t)]$**

To define the time-dependence of  $\{\sigma^\alpha(v_k, 0), \sigma^\beta(h_m, t)\}_+$  and  $[\sigma^\alpha(v_k, 0), \sigma^\beta(h_m, t)]$ , it is essential to establish time-dependence for  $\sigma^\beta(h_m, t)$  where  $\alpha, \beta \in \{0, x, y, z\}$  with  $\sigma^0 = \mathcal{I}_{2 \times 2}$ . To this end, we prove the following lemma.

**Lemma D.1.** *For an operator  $\sigma^\beta(h_m, t)$  satisfying the equation  $\dot{\sigma}^\beta(h_m, t) = i[\mathcal{H}, \sigma^\beta(h_m, t)]$ , (generator  $\mathcal{H}$  defined in Eq.3 in main manuscript), the solution would be  $\sigma^\beta(h_m, t) = e^{2i\mathcal{H}'t} \sigma^\beta(h_m, 0) \forall \beta \in \{0, x, y, z\}$  with*

$$\mathcal{H}' = \delta_{\beta \in \{x, y\}} (\mathcal{H} - \sum_l a_l \sigma^z(v_l, 0) - \sum_{j \neq m} b_j \sigma^z(h_j, 0) - \sum_{l, j \neq m} W_j^l \sigma^z(v_l, 0) \sigma^z(h_j, 0))$$

*Proof.*

$$\begin{aligned} \dot{\sigma}^\beta(h_m, t) &= i[\mathcal{H}, \sigma^\beta(h_m, t)] \\ &= i e^{i\mathcal{H}t} [\mathcal{H}, \sigma^\beta(h_m, 0)] e^{-i\mathcal{H}t} \\ &= i e^{i\mathcal{H}t} (b_m [\sigma^z(h_m, 0), \sigma^\beta(h_m, 0)] + \sum_l W_m^l [\sigma^z(v_l, 0) \sigma^z(h_m, 0), \sigma^\beta(h_m, 0)]) e^{-i\mathcal{H}t} \\ &= 2i \delta_{\beta \in \{x, y\}} e^{i\mathcal{H}t} (b_m \sigma^z(h_m, 0) \sigma^\beta(h_m, 0) + \sum_l W_m^l \sigma^z(v_l, 0) \sigma^z(h_m, 0) \sigma^\beta(h_m, 0)) e^{-i\mathcal{H}t} \\ &= 2i \delta_{\beta \in \{x, y\}} (b_m \sigma^z(h_m, 0) + \sum_l W_m^l \sigma^z(v_l, 0) \sigma^z(h_m, 0)) \sigma^\beta(h_m, t) \\ &= 2i \delta_{\beta \in \{x, y\}} (\mathcal{H} - \sum_l a_l \sigma^z(v_l, 0) - \sum_{j \neq m} b_j \sigma^z(h_j, 0) - \sum_{l, j \neq m} W_j^l \sigma^z(v_l, 0) \sigma^z(h_j, 0)) \sigma^\beta(h_m, t) \\ &= 2i \mathcal{H}' \sigma^\beta(h_m, t) \\ \sigma^\beta(h_m, t) &= e^{2i\mathcal{H}'t} \sigma^\beta(h_m, 0) \end{aligned}$$

□

**Lemma D.2.** *The explicitly time dependant forms of  $[\sigma^\alpha(v_k, 0), \sigma^\beta(h_m, t)]$  and  $\{\sigma^\alpha(v_k, 0), \sigma^\beta(h_m, t)\}_+$  are*

$$\begin{aligned} 1. \hat{\Theta}_{\alpha, \beta}(t) &= [\sigma^\alpha(v_k, 0), \sigma^\beta(h_m, t)] \\ &= -2i \text{Sin}(2W_m^k t) \det \begin{pmatrix} \delta_{\alpha z} & \delta_{\alpha \beta} & \delta_{\alpha \gamma} \\ 1 & \delta_{z \beta} & \delta_{z \gamma} \\ \delta_{\chi z} & \delta_{\chi \beta} & \delta_{\chi \gamma} \end{pmatrix} \hat{F} \sigma^\chi(v_k, 0) \sigma^\gamma(h_m, 0) \\ 2. \hat{\Phi}_{\alpha, \beta}(t) &= \{\sigma^\alpha(v_k, 0), \sigma^\beta(h_m, t)\}_+ \\ &= -2i \text{Sin}(2W_m^k t) \det \begin{pmatrix} \delta_{\alpha z} & \delta_{\alpha \beta} & \delta_{\alpha \gamma} \\ 1 & \delta_{z \beta} & \delta_{z \gamma} \\ \delta_{\chi z} & \delta_{\chi \beta} & \delta_{\chi \gamma} \end{pmatrix} \hat{F} \sigma^\chi(v_k, 0) \sigma^\gamma(h_m, 0) + 2e^{2i\mathcal{H}'t} \sigma^\alpha(v_k, 0) \sigma^\beta(h_m, 0) \end{aligned}$$

with  $\hat{F} = e^{2ib_m \sigma^z(h_m, 0)t} \prod_{l \neq k} e^{2iW_m^l \sigma^z(v_l, 0) \sigma^z(h_m, 0)t}$  being a unitary operator. For definition of  $\mathcal{H}'$  see Lemma. D.1. Here we restrict  $\alpha, \beta \in \{x, y, z\}$  as the commutation / anti-commutation relations with  $\mathcal{I}_{2 \times 2}$  are trivial.

*Proof.*

$$\begin{aligned} 1. \hat{\Theta}_{\alpha, \beta}(t) &= [\sigma^\alpha(v_k, 0), \sigma^\beta(h_m, t)] \\ &= [\sigma^\alpha(v_k, 0), e^{2i\mathcal{H}'t} \sigma^\beta(h_m, 0)] \quad \because \text{Lemma D.1} \\ &= e^{2ib_m \sigma^z(h_m, 0)t} \prod_{l \neq k} e^{2iW_m^l \sigma^z(v_l, 0) \sigma^z(h_m, 0)t} [\sigma^\alpha(v_k, 0), e^{2iW_m^k \sigma^z(v_k, 0) \sigma^z(h_m, 0)t} \sigma^\beta(h_m, 0)] \\ &= \hat{F} [\sigma^\alpha(v_k, 0), i \sigma^z(v_k, 0) \sigma^z(h_m, 0) \sigma^\beta(h_m, 0) \text{Sin}(2W_m^k t)] \\ &= -2i (\epsilon_{\alpha z \chi}) (\epsilon_{z \beta \gamma}) \text{Sin}(2W_m^k t) \hat{F} \sigma^\chi(v_k, 0) \sigma^\gamma(h_m, 0) \\ &= -2i \text{Sin}(2W_m^k t) \det \begin{pmatrix} \delta_{\alpha z} & \delta_{\alpha \beta} & \delta_{\alpha \gamma} \\ 1 & \delta_{z \beta} & \delta_{z \gamma} \\ \delta_{\chi z} & \delta_{\chi \beta} & \delta_{\chi \gamma} \end{pmatrix} \hat{F} \sigma^\chi(v_k, 0) \sigma^\gamma(h_m, 0) \end{aligned}$$

$$\begin{aligned}
2. \hat{\Phi}_{\alpha,\beta}(t) &= \{\sigma^\alpha(v_k, 0), \sigma^\beta(h_m, t)\}_+ \\
&= \{\sigma^\alpha(v_k, 0), e^{2i\mathcal{H}'t} \sigma^\beta(h_m, 0)\}_+ \quad \because \text{Lemma D.1} \\
&= [\sigma^\alpha(v_k, 0), e^{2i\mathcal{H}'t} \sigma^\beta(h_m, 0)] + e^{2i\mathcal{H}'t} \{\sigma^\alpha(v_k, 0), \sigma^\beta(h_m, 0)\}_+ \\
&= [\sigma^\alpha(v_k, 0), e^{2i\mathcal{H}'t} \sigma^\beta(h_m, 0)] + 2e^{2i\mathcal{H}'t} \sigma^\alpha(v_k, 0) \sigma^\beta(h_m, 0) \\
&= -2i \sin(2W_m^k t) \det \begin{pmatrix} \delta_{\alpha z} & \delta_{\alpha \beta} & \delta_{\alpha \gamma} \\ 1 & \delta_{z\beta} & \delta_{z\gamma} \\ \delta_{\chi z} & \delta_{\chi \beta} & \delta_{\chi \gamma} \end{pmatrix} \hat{\mathcal{F}} \sigma^\chi(v_k, 0) \sigma^\gamma(h_m, 0) + 2e^{2i\mathcal{H}'t} \sigma^\alpha(v_k, 0) \sigma^\beta(h_m, 0) \\
&\quad \because \text{Lemma D.2(1)}
\end{aligned}$$

□

**Lemma D.3.** As defined in Lemma D.2, if  $\hat{\Theta}_{\alpha,\beta}(t) = [\sigma^\alpha(v_k, 0), \sigma^\beta(h_m, t)]$  and  $\hat{\Phi}_{\alpha,\beta}(t) = \{\sigma^\alpha(v_k, 0), \sigma^\beta(h_m, t)\}_+$ , then  $\forall \alpha, \beta \in \{0, x, y, z\}$ ,  $\hat{\Theta}_{\alpha,\beta}(t)$  and  $\hat{\Phi}_{\alpha,\beta}(t)$  satisfies the following operator differential equations:

$$\begin{aligned}
1. \frac{1}{2} \left( \frac{\partial^2 \hat{\Theta}_{\alpha,\beta}(t)^\dagger \hat{\Theta}_{\alpha,\beta}(t)}{\partial t^2} \right) &= \delta_{\alpha \in \{x,y\}} \delta_{\beta \in \{x,y\}} (4W_m^k)^2 (\mathcal{I}_{2 \times 2} - \frac{\hat{\Theta}_{\alpha,\beta}(t)^\dagger \hat{\Theta}_{\alpha,\beta}(t)}{2}) \\
2. \frac{\partial^2 \hat{\Phi}_{\alpha,\beta}(t)^\dagger \hat{\Phi}_{\alpha,\beta}(t)}{\partial t^2} &= \delta_{\alpha \in \{x,y\}} \delta_{\beta \in \{x,y\}} (4W_m^k)^2 \hat{\Phi}_{\alpha,\beta}(t)^\dagger \hat{\Phi}_{\alpha,\beta}(t)
\end{aligned}$$

*Proof.*

- Using products like  $\hat{\Theta}_{\alpha,\beta}(t)^\dagger \hat{\Theta}_{\alpha,\beta}(t)$  ensures the unitary operator  $\mathcal{F}$  cancels. The satisfaction of (1) can thereafter be verified explicitly as:

$$\begin{aligned}
&\frac{1}{2} \left( \frac{\partial^2 \hat{\Theta}_{\alpha,\beta}(t)^\dagger \hat{\Theta}_{\alpha,\beta}(t)}{\partial t^2} \right) \\
&= 2\delta_{\alpha \in \{x,y\}} \delta_{\beta \in \{x,y\}} (\sigma^\chi(v_k, 0) \sigma^\gamma(h_m, 0))^2 \frac{\partial^2 (\sin^2(2W_m^k t) \mathcal{F}^\dagger \mathcal{F})}{\partial t^2} \mathcal{I}_{2 \times 2} \quad \because \text{Lemma D.2(1)} \\
&= \delta_{\alpha \in \{x,y\}} \delta_{\beta \in \{x,y\}} (4W_m^k) \frac{\partial \sin(4W_m^k t)}{\partial t} \mathcal{I}_{2 \times 2} \\
&= \delta_{\alpha \in \{x,y\}} \delta_{\beta \in \{x,y\}} (4W_m^k)^2 (1 - 2\sin^2(4W_m^k t)) \mathcal{I}_{2 \times 2} \\
&= \delta_{\alpha \in \{x,y\}} \delta_{\beta \in \{x,y\}} (4W_m^k)^2 (\mathcal{I}_{2 \times 2} - \frac{\hat{\Theta}_{\alpha,\beta}(t)^\dagger \hat{\Theta}_{\alpha,\beta}(t)}{2})
\end{aligned}$$

- Similarly (2) above can be verified explicitly too as follows

$$\begin{aligned}
& \frac{1}{2} \left( \frac{\partial^2 \hat{\Phi}_{\alpha,\beta}(t)^\dagger \hat{\Theta}_{\alpha,\beta}(t)}{\partial t^2} \right) \tag{D1} \\
&= \frac{1}{2} \left( \frac{\partial^2}{\partial t^2} (\hat{\Theta}_{\alpha,\beta}^\dagger(t) \hat{\Theta}_{\alpha,\beta}(t) + 2\sigma^\alpha(v_k, 0) \sigma^\alpha(h_m, 0) e^{-2i\mathcal{H}'t} \hat{\Theta}_{\alpha,\beta}(t)) \right) \quad \because \text{Lemma D.2(2)} \\
&= \frac{1}{2} \left( \frac{\partial^2}{\partial t^2} (\hat{\Theta}_{\alpha,\beta}^\dagger(t) \hat{\Theta}_{\alpha,\beta}(t)) \right) + \sigma^\alpha(v_k, 0) \sigma^\alpha(h_m, 0) \left( \frac{\partial^2}{\partial t^2} e^{-2i\mathcal{H}'t} \hat{\Theta}_{\alpha,\beta}(t) \right) \\
&= \frac{1}{2} \left( \frac{\partial^2}{\partial t^2} (\hat{\Theta}_{\alpha,\beta}^\dagger(t) \hat{\Theta}_{\alpha,\beta}(t)) \right) - 2i\epsilon_{\alpha z \chi} \epsilon_{z \beta \gamma} \sigma^\alpha(v_k, 0) \sigma^\alpha(h_m, 0) \\
&\quad \frac{\partial^2}{\partial t^2} (e^{-2i\mathcal{H}'t} \mathcal{F} \sigma^\chi(v_k, 0) \sigma^\gamma(h_m, 0) \text{Sin}(2W_m^k t)) \quad \text{see Lemma D.2(1) for } \mathcal{F} \\
&= \frac{1}{2} \left( \frac{\partial^2}{\partial t^2} (\hat{\Theta}_{\alpha,\beta}^\dagger(t) \hat{\Theta}_{\alpha,\beta}(t)) \right) - 2i\epsilon_{\alpha z \chi} \epsilon_{z \beta \gamma} \sigma^\alpha(v_k, 0) \sigma^\alpha(h_m, 0) \\
&\quad \frac{\partial^2}{\partial t^2} (\sigma^\chi(v_k, 0) \sigma^\gamma(h_m, 0) \text{Cos}(W_m^k t) \text{Sin}(2W_m^k t) + \epsilon_{z \chi \omega} \epsilon_{z \gamma \eta} \sigma^\omega(v_k, 0) \sigma^\eta(h_m, 0) \text{Sin}^2(2W_m^k t)) \\
&= \frac{1}{2} \left( \frac{\partial^2}{\partial t^2} (\hat{\Theta}_{\alpha,\beta}^\dagger(t) \hat{\Theta}_{\alpha,\beta}(t)) \right) - 2i\epsilon_{\alpha z \chi} \epsilon_{z \beta \gamma} \sigma^\alpha(v_k, 0) \sigma^\alpha(h_m, 0) \\
&\quad \frac{\partial^2}{\partial t^2} (\sigma^\chi(v_k, 0) \sigma^\gamma(h_m, 0) \text{Cos}(W_m^k t) \text{Sin}(2W_m^k t)) - \frac{1}{2} \left( \frac{\partial^2}{\partial t^2} (\hat{\Theta}_{\alpha,\beta}^\dagger(t) \hat{\Theta}_{\alpha,\beta}(t)) \right) \\
&= -2i\epsilon_{\alpha z \chi} \epsilon_{z \beta \gamma} \sigma^\alpha(v_k, 0) \sigma^\alpha(h_m, 0) \frac{\partial^2}{\partial t^2} (\sigma^\chi(v_k, 0) \sigma^\gamma(h_m, 0) \text{Cos}(W_m^k t) \text{Sin}(2W_m^k t)) \\
&= 2i\epsilon_{\alpha z \chi} \epsilon_{z \beta \gamma} \epsilon_{\alpha \chi \kappa} \epsilon_{\beta \gamma \omega} \frac{\partial^2}{\partial t^2} (\sigma^\kappa(v_k, 0) \sigma^\omega(h_m, 0) \text{Cos}(W_m^k t) \text{Sin}(2W_m^k t)) \\
&= -2i \frac{\partial^2}{\partial t^2} (\sigma^z(v_k, 0) \sigma^z(h_m, 0) \text{Cos}(W_m^k t) \text{Sin}(2W_m^k t)) \\
&= \frac{1}{2} \frac{\partial^2}{\partial t^2} (-2i \sigma^z(v_k, 0) \sigma^z(h_m, 0) \text{Sin}(4W_m^k t)) \tag{D2} \\
&= -(4W_m^k)^2 \hat{\Phi}_{\alpha,\beta}(t)^\dagger \hat{\Theta}_{\alpha,\beta}(t)
\end{aligned}$$

where the last equality follows from Eq.D1 and Eq.D2 which shows  $\frac{1}{2} \left( \frac{\partial^2 \hat{\Phi}_{\alpha,\beta}(t)^\dagger \hat{\Theta}_{\alpha,\beta}(t)}{\partial t^2} \right) = \frac{1}{2} \frac{\partial^2}{\partial t^2} (-2i \sigma^z(v_k, 0) \sigma^z(h_m, 0) \text{Sin}(4W_m^k t))$  thereby implying  $\hat{\Phi}_{\alpha,\beta}(t)^\dagger \hat{\Theta}_{\alpha,\beta}(t) = -2i \sigma^z(v_k, 0) \sigma^z(h_m, 0) \text{Sin}(4W_m^k t)$

□

#### Appendix E: Relationship between $C_{\sigma^\alpha, \sigma^\beta}(\kappa_1, \kappa_2, \vec{X}, t)$ and $C_{\sigma^\alpha, \sigma^\beta}(0, 0, \vec{X}, t)$

**Lemma E.1.**  $\sigma^\alpha f(\sigma^z)(\sigma^\alpha)^\dagger = f(-\sigma^z) \quad \forall \alpha \in \{x, y\}$

*Proof.*

$$\begin{aligned}
& \sigma^\alpha \sigma^z (\sigma^\alpha)^\dagger \\
&= i \sigma^\alpha \epsilon_{z \alpha k} \sigma^k = i^2 \epsilon_{z \alpha k} \epsilon_{\alpha k \omega} \sigma^\omega = i^2 \delta_{\omega z} \sigma^\omega = -\sigma^z \quad \because (\alpha \in \{x, y\}) \\
& \sigma^\alpha f(\sigma^z)(\sigma^\alpha)^\dagger \\
&= \sigma^\alpha [\beta_0 + \beta_1 \sigma^z + \beta_2 (\sigma^z)^2 + \dots] (\sigma^\alpha)^\dagger \\
&= \beta_0 \sigma^\alpha (\sigma^\alpha)^\dagger + \beta_1 \sigma^\alpha \sigma^z (\sigma^\alpha)^\dagger + \beta_2 [\sigma^\alpha \sigma^z (\sigma^\alpha)^\dagger]^2 + \dots \\
&= \beta_0 - \beta_1 \sigma^z + \beta_2 (\sigma^z)^2 - \beta_3 (\sigma^z)^3 + \dots \\
&= f(-\sigma^z)
\end{aligned}$$



□

**Lemma E.2.** For a diagonal matrix  $A$  and an off-diagonal matrix  $B$ ,  $Tr(AB) = 0$   
 Given:  $B_i^k = 0 \quad \forall \quad i = k$  and  $A_i^k = a_i \delta_i^k$

*Proof.*

$$Tr(AB) = \sum_i (AB)_i^i = \sum_i A_i^k B_i^k = \sum_i a_i \delta_i^k B_i^k = \sum_i a_i B_i^i = 0$$

□

**Lemma E.3.**

$$C_{\sigma^\alpha, \sigma^\beta}(\kappa_1, \kappa_2, \vec{X}, t) = \langle \tilde{\sigma}^\alpha(v_k, 0) \tilde{\sigma}^\beta(h_m, t) \tilde{\sigma}^\alpha(v_k, 0) \tilde{\sigma}^\beta(h_m, t) \rangle = C_{\sigma^\alpha, \sigma^\beta}(0, 0, \vec{X}, t) + |\kappa_1|^2 |\kappa_2|^2 + |\kappa_2|^2 + |\kappa_1|^2$$

where  $\alpha, \beta \in \{x, y\}$

*Proof.* Let us define  $\tilde{U}_1(0) = U_1(0) - \kappa_1 \mathcal{I}$  and  $\tilde{U}_2(0) = U_2(0) - \kappa_2 \mathcal{I}$  where  $U_1(0)$  and  $U_2(0)$  are two unitary operators as defined in the main manuscript

$$\begin{aligned} & \langle \tilde{U}_1(0)^\dagger \tilde{U}_2(t)^\dagger \tilde{U}_1(0) \tilde{U}_2(t) \rangle \\ &= \langle U_1(0)^\dagger U_2(t)^\dagger U_1(0) U_2(t) \rangle + |\kappa_1|^2 |\kappa_2|^2 \\ & \quad - \kappa_2 \langle U_1(0)^\dagger U_2(t)^\dagger U_1(0) \rangle - \kappa_1 \langle U_1(0)^\dagger U_2(t)^\dagger U_2(t) \rangle \\ & \quad - \kappa_2^* \langle U_1(0)^\dagger U_1(0) U_2(t) \rangle - \kappa_1^* \langle U_2(t)^\dagger U_1(0) U_2(t) \rangle \\ & \quad + |\kappa_2|^2 \langle U_1^\dagger(0) U_1(0) \rangle + |\kappa_1|^2 \langle U_2^\dagger(t) U_2(t) \rangle + \kappa_1^* \kappa_2 \langle U_2^\dagger(t) U_1(0) \rangle \\ & \quad + \kappa_1 \kappa_2^* \langle U_1^\dagger(0) U_2(t) \rangle + \kappa_1^* \kappa_2^* \langle U_1(0) U_2(t) \rangle + \kappa_1 \kappa_2 \langle U_1^\dagger(0) U_2^\dagger(t) \rangle \\ & \quad - \kappa_1 |\kappa_2|^2 \langle U_1(0)^\dagger \rangle - |\kappa_1|^2 \kappa_2 \langle U_2(t)^\dagger \rangle - \kappa_1^* |\kappa_2|^2 \langle U_1(0) \rangle - |\kappa_1|^2 \kappa_2^* \langle U_2(t) \rangle \end{aligned} \quad (E1)$$

Let us now substitute  $U_1(0) = \sigma^\alpha(v_k, 0)$  and  $U_2(t) = \sigma^\beta(h_m, t)$  in Eq. E1

By definition,

$$\langle \sigma^\alpha(v_k, 0) \sigma^\beta(h_m, t) \sigma^\alpha(v_k, 0) \sigma^\beta(h_m, t) \rangle = C_{\sigma^\alpha, \sigma^\beta}(0, 0, \vec{X}, t) \quad (E2)$$

Also one can show the following:

a)

$$\begin{aligned} & \langle \sigma^\alpha(v_k, 0) \sigma^\beta(h_m, t) \sigma^\alpha(v_k, 0) \rangle \\ &= Tr(\rho_{th}(\vec{X}, v_k, h_m) \sigma^\alpha(v_k, 0) \sigma^\beta(h_m, t) \sigma^\alpha(v_k, 0)) \\ &= Tr(\sigma^\alpha(v_k, 0) \rho_{th}(\vec{X}, v_k, h_m) \sigma^\alpha(v_k, 0) \sigma^\beta(h_m, t)) \\ &= Tr(\rho_{th}(\vec{X}, -v_k, h_m) e^{iHt} \sigma^\beta(h_m, 0) e^{-iHt}) \quad \text{See Lemma E.1 and Lemma D.1} \\ &= Tr(e^{-iHt} \rho_{th}(\vec{X}, -v_k, h_m) e^{iHt} \sigma^\beta(h_m, 0)) \\ &= Tr(\rho_{th}(\vec{X}, -v_k, h_m) \sigma^\beta(h_m, 0)) \quad \because e^{iHt} \text{ \& } \rho \text{ are diagonal} \\ &= 0 \quad \text{See Lemma E.2} \end{aligned} \quad (E3)$$

b)

$$\begin{aligned}
& \langle \sigma^\beta(h_m, t) \sigma^\alpha(v_k, 0) \sigma^\beta(h_m, t) \rangle \\
&= Tr(\rho_{th}(\vec{X}, v_k, h_m) \sigma^\beta(h_m, t) \sigma^\alpha(v_k, 0) \sigma^\beta(h_m, t)) \\
&= Tr(\sigma^\beta(h_m, t) \rho_{th}(\vec{X}, v_k, h_m) \sigma^\beta(h_m, t) \sigma^\alpha(v_k, 0)) \\
&= Tr(e^{iHt} \sigma^\beta(h_m, 0) e^{-iHt} \rho_{th}(\vec{X}, v_k, h_m) e^{iHt} \sigma^\beta(h_m, 0) e^{-iHt} \sigma^\alpha(v_k, 0)) \\
&= Tr(e^{iHt} \sigma^\beta(h_m, 0) \rho_{th}(\vec{X}, v_k, h_m) \sigma^\beta(h_m, 0) e^{-iHt} \sigma^\alpha(v_k, 0)) \quad \because e^{iHt} \text{ \& } \rho \text{ are diagonal} \\
&= Tr(e^{iHt} \rho_{th}(\vec{X}, v_k, -h_m) e^{-iHt} \sigma^\alpha(v_k, 0)) \quad \text{See Lemma E.1} \\
&= Tr(\rho_{th}(\vec{X}, v_k, -h_m) \sigma^\alpha(v_k, 0)) \quad \because e^{iHt} \text{ \& } \rho \text{ are diagonal} \\
&= 0 \quad \text{See Lemma E.2}
\end{aligned} \tag{E4}$$

c)

$$\begin{aligned}
& \langle \sigma^\alpha(v_k, 0) \sigma^\beta(h_m, t) \sigma^\beta(h_m, t) \rangle \\
&= \langle \sigma^\alpha(v_k, 0) \rangle \\
&= Tr(\rho_{th}(\vec{X}, v_k, h_m) \sigma^\alpha(v_k, 0)) \\
&= 0 \quad \text{See Lemma E.2}
\end{aligned} \tag{E5}$$

d)

$$\begin{aligned}
& \langle \sigma^\alpha(v_k, 0) \sigma^\alpha(v_k, 0) \sigma^\beta(h_m, t) \rangle = \langle \sigma^\beta(h_m, t) \rangle \\
&= Tr(\rho_{th}(\vec{X}, v_k, h_m) \sigma^\beta(h_m, t)) \\
&= 0 \quad \text{See Lemma E.2}
\end{aligned} \tag{E6}$$

e)

$$\begin{aligned}
& \langle \sigma^\beta(h_m, t) \sigma^\alpha(v_k, 0) \rangle = Tr(\rho_{th}(\vec{X}, v_k, h_m) \sigma^\beta(h_m, t) \sigma^\alpha(v_k, 0)) \\
&= Tr(\rho_{th}(\vec{X}, v_k, h_m) e^{2iHt} \sigma^\beta(h_m, 0) \sigma^\alpha(v_k, 0)) \quad \text{See Lemma D.1} \\
&= 0 \quad \text{See Lemma E.2}
\end{aligned} \tag{E7}$$

Here  $\rho e^{2iHt}$  is diagonal,  $\sigma^\beta(h_m, 0) \sigma^\alpha(v_k, 0)$  is off-diagonal

Similarly we can show  $\langle \sigma^\alpha(v_k, 0) \sigma^\beta(h_m, t) \rangle = 0$

$$\langle \sigma^\alpha(v_k, 0) \rangle = \langle \sigma^\beta(h_m, t) \rangle = 0 \quad \text{See Lemma E.2}$$

Substituting the results of Eq.E2, E3, E4, E5, E6, E7 in Eq.E1 establishes the claim of the lemma

□

## Appendix F: Training of TFIM and c-TFIM

The figure Fig.4 and Fig.5 depicts the training of RBM network  $G$  for TFIM and c-TFIM model respectively. It shows the variation of Energy accuracy with epochs for training  $G$ . For each training process parameters of RBM are initialized randomly. Learning rate used is 0.001 and  $(n, p) = (4, 4)$  in network  $G$ . The convergence threshold set is  $1e - 3$ . The relative error in the converged state is less than 0.05%. Energy accuracy =  $\langle \psi(\vec{X}) | H | \psi(\vec{X}) \rangle - \lambda_0$  where Hamiltonian  $H$  is that of the driver (TFIM or c-TFIM) and the state  $\psi(\vec{X})$  is the ansatz for the corresponding ground state.  $\lambda_0$  is the smallest eigenvalue (true ground state energy) of the Hamiltonian.

For Fig. 3 - (d, e, g, h) in the main manuscript, to obtain each point, we average over all pairs of visible and hidden indices for  $I(v_k, h_m)$  and  $\eta(\vec{X})$  (i.e.  $k = \{1, 2, 3, 4\}$ ,  $m = \{1, 2, 3, 4\}$  implying 16 pairs) and another averaging over a sample of 100 best-converged points obtained from the training of 1000 randomly initialized networks.

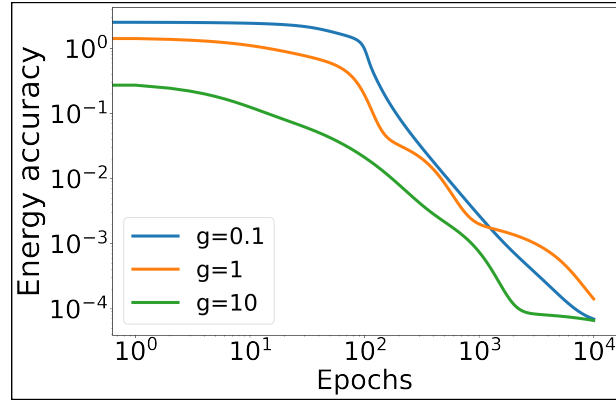


FIG. 4. TFIM

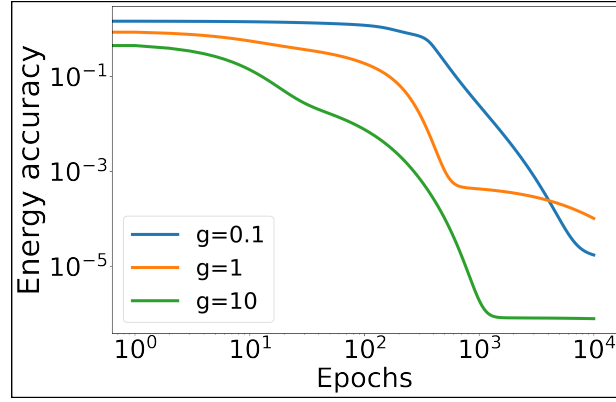


FIG. 5. c-TFIM

### Appendix G: Von-Neumann Entropy of TFIM and c-TFIM

The Von Neumann Entropy of the ground state for (a) TFIM (Fig. 6) and (b) c-TFIM (Fig. 7) models across the central cut (passing through the mid-point of the chain) for varying system sizes ( $N$ ) is depicted. The ground state of the TFIM model obeys the Area-Law (and hence is constant in 1D) while that of c-TFIM follows the Volume-Law scaling of entanglement entropy and increases proportionally to the increasing size of the chain.

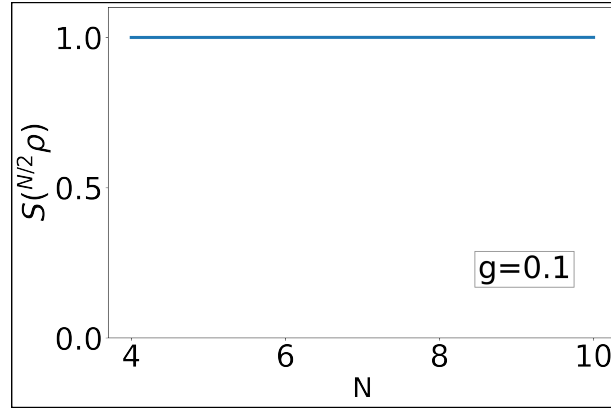


FIG. 6. TFIM

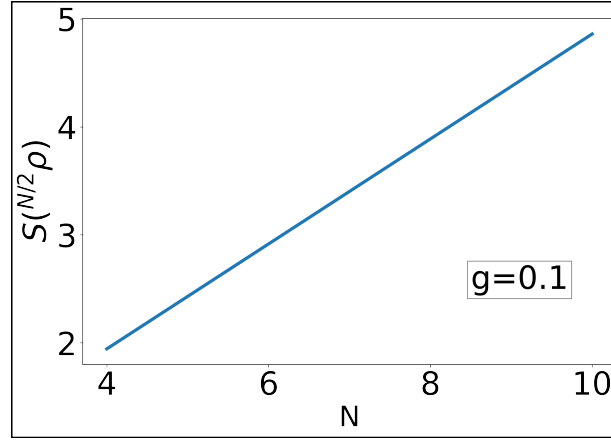


FIG. 7. c-TFIM

#### Appendix H: Fisher Information of TFIM and c-TFIM

The variation of the largest eigenvalue of the Fisher Information Matrix with  $g$  for (a) TFIM and (b) c-TFIM models. The color gradation depicts the increasing value of  $g$  from red to blue. Each point on the Fig. 8 and 9 is obtained by averaging over several best-converged points after training 1000 randomly initialized RBMs. A similar procedure was followed for all plots in Fig.3 in main manuscript

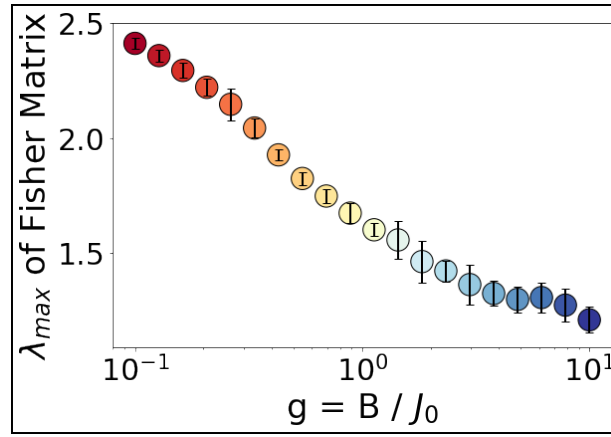


FIG. 8. TFIM

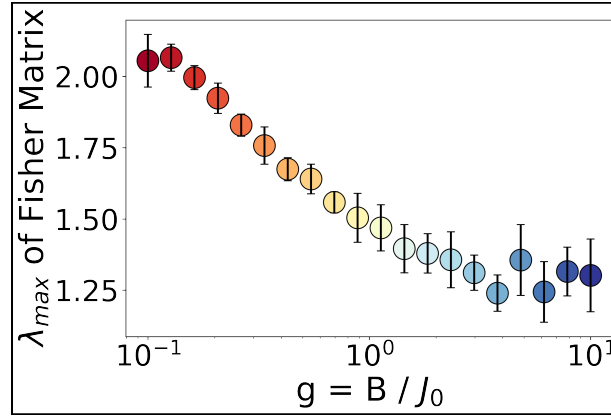


FIG. 9. c-TFIM